A FORNBERG-LIKE METHOD FOR THE NUMERICAL CONFORMAL MAPPING OF BOUNDED MULTIPLY CONNECTED DOMAINS

A Thesis by

Everett Kropf

Bachelor of Arts, Wichita State University, 2007

Submitted to the Department of Mathematics and Statistics
and the faculty of the Graduate School of
Wichita State University
in partial fulfillment of
the requirements for the degree of
Master of Science

May 2009

A FORNBERG-LIKE METHOD FOR THE NUMERICAL CONFORMAL MAPPING OF BOUNDED MULTIPLY CONNECTED DOMAINS

The following faculty members have examined the final copy of this thesis for form and content, and recommend that it be accepted in partial fulfullment of the requirement for the degree of Master of Science with a major in Applied Mathematics.

Thomas K. DeLillo,	Committee Chair
Alan R. Elcrat,	Committee Member
Ikramuddin Ahmed,	Committee Member

ABSTRACT

A new Fornberg-like method is presented for computing conformal maps from the interior of the unit disk with $m-1$ circular holes to the interior of a smooth closed curve with $m-1$ holes bounded by smooth curves. The method is a Newton-like method for computing the boundary correspondences and the conformal moduli (centers and radii of the circles). The inner linear systems are derived from conditions for analytic extension of functions defined on the circles to the interior domain. These systems are N-point trigonometric discretizations of the identity plus a compact operator and are solved efficiently with the conjugate gradient method at a cost of $\mathrm{O}(N^2)$ per step. Two formulations of the map are given: the first uses a disk with circular holes, and the second uses an annulus with circular holes. Some numerical examples are given.

TABLE OF CONTENTS

Chapter Page

1 INTRODUCTION 1
1.1 Basic theorems 3
1.2 Linear operators 7
1.3 Fornberg's method for the simply connected case 10
1.4 The conjugate gradient method 13

2 THE GENERALIZED METHOD 15
2.1 The circle map problem 15
2.2 Form of the map 15
2.3 Analyticity conditions 16
2.4 Linearization 20
2.5 Normalization conditions 21
2.6 Discretization and matrix formation 21
2.7 Analysis of the linear system 24
2.8 Numerical examples 26

3 THE ANNULUS WITH CIRCULAR HOLES CASE 32
3.1 The circle map problem revisited 32
3.2 Form of the map 32
3.3 Analyticity conditions 33
3.4 Linearization 34
3.5 Discretization and matrix formation 34
3.6 Analysis of the linear system 36
3.7 Numerical examples 38

4 CONCLUSION 41
4.1 Concluding remarks 41
4.2 Future work 41

LIST OF REFERENCES 43

APPENDICES 46

A The Matrix P 47
B The Algorithm 52

LIST OF TABLES

Table Page

2.1 Identity map accuracy. 27

2.2 Convergence of the Newton iteration. 28

2.3 Number of zero eigenvalues in the numeric examples. 31

3.4 Identity map accuracy. 38

3.5 Number of zero eigenvalues in the examples. 40

LIST OF FIGURES

Figure Page

1.1 Circle domain D and target domain Ω. 5

1.2 A simple CG implementation in MATLAB. 13

2.3 Eigenvalues of A grouped around 1 for $m = 7$ and $N = 128$. 26

2.4 An identity map. 27

2.5 A simple ellipse target region. 28

2.6 Inverted ellipse. 29

2.7 Spline outer boundary. 30

2.8 Submatrix eigenvalue plots. 30

2.9 Connectivity $m = 7$. 31

3.10 An identity map. 38

3.11 Spline outer boundary. 39

3.12 Connectivity $m = 6$. 39

A.1 MATLAB code for submatrix (A.51). 50

A.2 MATLAB code for submatrix (A.52). 51

A.3 MATLAB code to produce submatrix (A.53). 51

B.1 Forming the matrix D. 53

B.2 Forming the matrix A and solving the linear system. 54

B.3 Applying the Newton updates. 54

B.4 Setting the Fourier coefficients and forming the map. 54

B.5 The map evaluation function. 55

CHAPTER 1

INTRODUCTION

In [8] Fornberg proposed a method for computing the conformal map from the interior of the unit disk to the interior of a smooth, closed curve. It was a Newton-like method for computing the boundary correspondence. An inner linear system was derived for the Newton updates based on the condition that the negatively indexed Fourier (Taylor) coefficients of the (periodic) boundary values must be 0 for the function to be analytic inside the disk. The map f was normalized by fixing $f(0)$ and one boundary point, $f(1)$. Fornberg found that the inner linear systems could be solved very efficiently using the conjugate gradient method with matrix-vector multiplication, based on fast Fourier transforms and N-point trigonometric interpolation, costing $O(N \log N)$. Widlund [23] showed that the inner linear systems were in fact the discretization of the identity plus a compact (intergal) operator and that the conjugate gradient method therefore converges superlinearly; see also [19]. This set-up was extended to the ellipse [4, 5], the doubly connected [7], and the unbounded multiply connected [6, 3] case. To carry out these extensions, conditions on the Fourier/Laurent coefficients are derived that guarantee analytic extension of functions defined on the boundaries to the interior of the (circular) computational domains. For multiply connected regions, the conformal moduli (centers and radii) of the circular computational domains must also be computed, along with the correspondences of each of the boundaries. Once again, Newton-like methods are used and the attractive feature that the inner linear systems are discretization of the identity plus a compact operator is preserved. Wegmann has developed similar methods based on Riemann-Hilbert problems; see [20, 21].

Other methods for the multiply connected case have been developed. In [18], Wang has implemented the Koebe method [11] for the circle maps using both the exterior simply connected methods of Wegmann and of Fornberg [7] to successively map the exterior of each boundary component to the exterior of a disk. Prosnak has developed a linearly convergent projection method for this mapping problem; see [12, 16, 22]. The book [15] gives many applications of this method to problems in fluid dynamics. The reader can find more references for the multiply connected case in [6, 21, 22].

The interested reader is referred to [9, 11, 22] for introductions to the numerical methods for conformal mapping. Most methods for numerical conformal mapping compute the conformal moduli and the boundary correspondences between the target (physical) domains and some canonical (computational) domain. Canonical domains whose boundaries are circles are popular alternatives, since the fast Fourier transform (FFT) can be applied.

In this thesis the bounded (interior) case is developed. A new Fornberg-like method for computing conformal maps from the interior of the unit disk with $m-1$ circular holes to the interior of a smooth closed curve with $m-1$ holes bounded by smooth curves is presented. The new method is a revision of the similar method for the unbounded (exterior) case presented in [3]. (The method in [3], was a "symmetrized" version of the method presented in [6].) As in [3], the attractive features of the inner systems are preserved. We first present a generalized case in which the unit disk with circular holes is the computational domain; the normalization of the map is done by fixing a point in the domain and a point on the boundary. Also developed is a case in which the annulus with circular holes is the computational domain. Although it can be shown that analytically the domains used in the two cases are equivalent, provided they share the same conformal moduli, we discover that the generalized case is in general numerically more advantageous. Numerical examples for both cases are presented.

Chapter 1 provides an introductory look at some basic theorems; it also includes a short exposition on Fornberg's original method for the simply connected case. Chapter 2

contains the development of the generalized case, along with numerical examples. Chapter 3 presents the annulus with circular holes case, again with numerical examples. Chapter 4 provides a short summary and notes on possible future work. Appendix A contains a more detailed discussion, with algorithms, of some matrices used in the formulation of both cases. Appendix B is an overview of the algorithm used in the general case, with MATLAB code; the algorithm for the annulus case is similar and is not presented.

1.1 Basic theorems

A conformal map from one region in the complex z-plane to another region in the complex w-plane is a one-to-one analytic function $w = f(z)$ such that $f'(z) \neq 0$. Therefore, for small h, $f(z+h) \approx f(z) + f'(z)h$, and so locally f takes a small circle centered at z, translates the center to $f(z)$, rotates the circle by $\arg f'(z)$, and multiplies the radius by $|f'(z)|$. From this it is easy to see that a conformal map preserves the angles of intersection of any two smooth curves.

For the simply connected regions, the Riemann Mapping Theorem guarantees the existence of the (inverse of the) mapping function from the unit disk to the region; see, e.g., [1].

Theorem 1.1 (Riemann mapping theorem)**.** *Let Ω be a simply connected region which is not the whole plane or the Riemann sphere, and let a be a point of Ω. Then there exists in Ω a unique analytic function f satisfying the conditions*

$$f(a) = 0 \quad \textit{and} \quad f'(a) > 0,$$

and assuming every value in the unit disk $D = \{w : |w| < 1\}$ exactly once.

Therefore any simply connected region on the Riemann sphere is conformally equivalent to the whole plane plus the point at infinity, the plane, or the unit disk. In the later case the map is unique up to self maps of the disk, that is, up to three real parameters.

In this thesis we will mainly be concerned with maps for bounded regions with finite connectivity $m > 2$. This definition of multiply connected regions is given in, e.g., [1].

Definition 1.1. *A region Ω which is not simply connected is said to be multiply connected. More precisely, Ω is said to have connectivity m if the complement of Ω has exactly m simply connected components.*

Another way to say this is that a region of connectivity m arises from punching m holes in the Riemann sphere.

In order to clarify the existence and uniqueness for the conformal map $w = f(z)$ for the multiply connected case, let us first consider unbounded regions containing infinity. Let f be conformal map f from the complement, D, of m closed nonintersecting disks, D_ν, onto a region Ω which is exterior to m nonintersecting smooth Jordan curves, $\Gamma_\nu, 1 \leq \nu \leq m$. (Figure 1.1 shows both the computational circle domain and the target domain for the bounded case.) The following theorem (actually stated for f^{-1} in [11, 17.1b]) establishes the existence and uniqueness of the circle map under suitable normalization conditions.

Theorem 1.2. *Let Ω be a region of connectivity $m \geq 2$ in the extended complex plane such that $\infty \in \Omega$. Then there exists a unique circular region D of connectivity n and a unique one-to-one analytic function f in D satisfying*

$$f(z) = z + O(1/z) \quad \textit{for} \quad z \approx \infty,$$

such that $f(D) = \Omega$.

In this thesis D_1 will be the exterior of the unit disk, and $D_\nu, \nu = 2, \ldots, m$ will be non-overlapping disks in the interior of the unit disk with boundary circles C_ν. Then D is the bounded region $\mathbb{C} - \overline{D}_1$ (the interior of the unit disk) minus the disks $D_\nu, \nu = 2, \ldots, m$. Correspondingly Ω will be the bounded region interior to an outer boundary Γ_1 and exterior to the inner boundaries $\Gamma_\nu, \nu = 2, \ldots, m$. In this case the mapping function $w = f(z)$ is uniquely determined up to self maps of the unit disk, or equivalently, say, by fixing $w_0 = f(z_0)$ for $z_0 \in D$ and $w_0 \in \Omega$ and $f(1) \in \Gamma_1$. This existence and uniqueness for the bounded case can be seen from Theorem 1.2 as follows. Map Ω to an unbounded domain by $1/(w - w_0)$. A unique conformally equivalent unbounded circle domain is then given by Theorem 1.2. Let

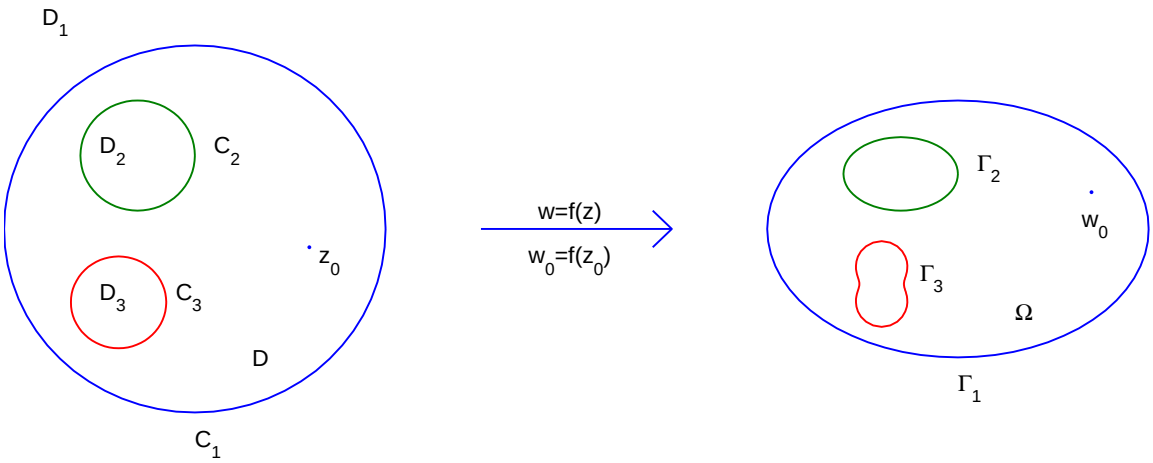

Figure 1.1: Computational circle domain D and target "physical" domain Ω for the bounded, multiply connected map $w = f(z)$ with $f(D) = \Omega$, $f(z_0) = w_0$, and $f(C_\nu) = \Gamma_\nu, \nu = 1, \ldots, m$ for connectivity $m = 3$.

Γ_1 map to the circle C_1' with center c_1' and radius r_1'. Then $r_1'/(z - c_1'))$ maps the exterior region to the interior of the unit disk D_1 with ∞ mapped to 0. A unique self-map of the unit disk taking 0 to z_0 and fixing a boundary point gives the unique bounded map between the bounded circle domain and the bounded domain Ω. The circles C_ν, $\nu = 2, \ldots, m$ are therefore uniquely determined by Ω and must be computed as part of the problem of finding f.

To find the C_ν's, it is sufficient to find their centers c_ν and radii ρ_ν for $\nu = 2, \ldots, m$. This amounts to finding $3m-3$ real parameters. Not all of these parameters are independent. As shown in [11, 14], two m-connected domains are conformally equivalent if and only if they have the same *conformal moduli*. We will give a specific geometrical meaning to the moduli related to the centers and radii of the circles. The moduli can be determined by maps to certain standard canonical domains. For instance, any m connected domain can be mapped to an annulus with $m - 1$ concentric circular slits. For $m = 2$ (no slits), two annuli are conformally equivalent if and only if the ratios of their outer to inner radii are equal. This ratio is the conformal modulus of the class of doubly connected domains which can be mapped to the annulus. If the outer radius is 1, we may take the inner radius ρ_2 as the

modulus (instead of $1/\rho_2$). For $m = 3$ the annulus has one circular slit. The annular domain is uniquely determined up to a rotation. Therefore the tip of the slit may be placed on the x-axis, the slit is then determined by its radius and its length. And so for $m = 3$ there are $3m - 6 = 3$ conformal moduli, ρ_2, and the length and radius of the slit. For $m \geq 4$ each new slit adds three new moduli, the angle of its tip, its radius, and its length. Thus, for $m > 2$ there are $3m - 6$ conformal moduli. For this thesis we may take the canonical domain as an annulus with circular holes. Then, for $m = 3$, the center and radius of the first hole may be taken as $c_3 > 0$ and ρ_3, and the $3m - 6 = 3$ conformal moduli are ρ_2, c_3, ρ_3. Again each new hole adds three more real parameters, the real and imaginary parts of its center and its radius. The annulus with circular holes is therefore uniquely determined (up to a rotation) by the target domain Ω. There is also a unique self-map of the unit disk to the original disk with holes $D_\nu, \nu = 2, \ldots, m$ when, e.g., $w_0 = f(z_0)$ and $f(1)$ are fixed. In this case, we must determine the $3m - 3$ real parameters given by $c_\nu, \rho_\nu, \nu = 2, \ldots, m$. The moduli determine $3m - 6$ parameters and fixing $f(1)$ and $f(z_0) = w_0$ determine the other 3 parameters. We will formulate our method for both the disk with circular holes and the annulus with circular holes, and discuss the discuss the numerical advantages of each case.

The other part of the calculation of f involves finding the correspondences between the related boundaries $f(C_\nu) = \Gamma_\nu$. The Osgood-Carathódory Theorem allows the map to be continuously extended to the boundary for regions bounded by sufficient smooth, e.g., Jordan, curves. The boundary correspondence functions can then be defined. Once the conformally equivalent circle domain and the boundary correspondences are known, the map can be computed at any interior point by using a series expansion on the Cauchy integral formula,

$$f(z) = \frac{1}{2\pi i} \int_C \frac{f(\zeta)}{\zeta - z}\, d\zeta = \frac{1}{2\pi i} \int_{C_1} \frac{\gamma_1(S_1(\theta))}{\zeta - z}\, d\zeta - \frac{1}{2\pi i} \sum_{\nu=2}^{m} \int_{C_\nu} \frac{\gamma_\nu(S_\nu(\theta))}{\zeta - z}\, d\zeta,$$

with $\zeta = c_\nu + \rho_\nu e^{i\theta}$, as explained below.

Theorem 1.3 (Osgood-Carathéodory)**.** *Let Ω be a Jordan region, and let f be a conformal map of Ω onto the open unit disk D. Then f can be extended to a one-to-one analytic map of the closure of Ω onto the closure of D.*

The boundaries of the circular disks D_ν are the circles C_ν with centers c_ν and radii ρ_ν, and are parametrized by $C_\nu(\theta) := z_\nu + \rho_\nu e^{i\theta}$. The boundary of D is thus $C = C_1 - C_2 - \cdots - C_m$.[1] The boundary of Ω is $\Gamma = \Gamma_1 - \Gamma_2 - \cdots - \Gamma_m$, where the boundaries Γ_ν are parametrized by S, e.g., arclength, $\Gamma_\nu : \gamma_\nu = \gamma_\nu(S)$. For smooth γ_ν, f extends smoothly to the boundary $f(C_\nu) = \Gamma_\nu$. The values of f on C will determine f everywhere. The *circle map problem* is, thus, to find the boundary correspondences $S = S_\nu(\theta)$ and the conformal moduli c_ν, ρ_ν such that

$$f(c_\nu + \rho_\nu e^{i\theta}) = \gamma_\nu(S_\nu(\theta)), \quad 1 \le \nu \le m,$$

where $f(z)$ is analytic for $z \in D$ and has the normalization $f(z_0) = w_0 \in \Omega$ and $f(1) \in \Gamma_1$ given.

1.2 Linear operators

Some operators on the space of periodic functions for the analysis of the linear systems will be needed. Presented here is a quick definition of some of these standard operators given in [19] and [7].

Let f be a 2π-periodic function in $L^2[0, 2\pi]$. If f is represented by a Fourier series

$$f(\theta) = \sum_{k=-\infty}^{\infty} a_k e^{ik\theta}, \tag{1.1}$$

then the conjugation operator K is given by

$$Kf(\theta) = \sum_{k=-\infty}^{-1} i a_k e^{ik\theta} - \sum_{k=1}^{\infty} i a_k e^{ik\theta}.$$

[1] Note the subtraction here indicates the orientation of the boundary, *i.e.*, counterclockwise for positive orientation, not the relative compliment of the boundary sets.

The conjugation operator can also be represented as a singular integral operator,

$$Kf(\theta) = \frac{1}{2\pi}\, PV \int_0^{2\pi} f(\phi) \cot\left(\frac{\theta-\phi}{2}\right)\, d\phi,$$

where PV denotes the Cauchy principal value. Let J be the operator

$$Jf(\theta) = \frac{1}{2\pi}\int_0^{2\pi} f(\theta)\, d\theta = a_0$$

with the coefficient a_0 of (1.1).

It will also help to make use of the discretization of the above operators. Consider an even number $N = 2M$ and let

$$\theta_k = \frac{2\pi k}{N}, \qquad k = 0, 1, \cdots, N-1.$$

Define $\underline{f} := f(\underline{\theta})$ where

$$\underline{\theta} = (\theta_0, \cdots, \theta_{N-1})^T, \quad f_k = f(\theta_k), \quad \underline{f} = (f_0, \cdots, f_{N-1})^T$$

and the discrete Fourier coefficients

$$\hat{a}_k = \frac{1}{N}\sum_{j=0}^{N-1} f_j e^{-i2\pi jk/N}.$$

The trigonometric polynomial interpolating f is then given by

$$T_N f(\theta) = \sum_{k=-M+1}^{M-1} \hat{a}_k e^{ik\theta} + \hat{a}_M \cos(M\theta),$$

which takes values f_k at θ_k, $k = 0,\ 1,\ \cdots,\ N-1$. The discrete conjugation is given by

$$K_N f(\theta) = \sum_{k=-M+1}^{-1} i\hat{a}_k e^{ik\theta} - \sum_{k=1}^{M-1} i\hat{a}_k e^{ik\theta},$$

and the discretization of the operator J is given by

$$J_N f = \hat{a}_0 - \hat{a}_M \cos(M\theta).$$

An operator P_- will also be put to use in the subsequent; this operator is given by

$$P_- f = \frac{1}{2}\left(I - iK + J\right) f = \sum_{k=0}^{\infty} a_k e^{ik\theta}$$

whose discrete form is

$$P_{-,N} f = \frac{1}{2}\left(T_N - iK_N + J_N\right) f.$$

Since the values of the functions $K_N f$ and $P_{-,N} f$ depend on the values $f(\theta_k)$ of f at the points θ_k, these operators can be represented as matrices. If the $N \times N$ discrete Fourier transform matrix is denoted by

$$F := [e^{-i2\pi jk}], \qquad j,k = 0, \cdots, N-1,$$

then

$$\frac{1}{N} F^H F = \frac{1}{N} F F^H = I_N,$$

where H is the Hermitian transpose and I_N is the N-by-N identity matrix. If the discrete Fourier coefficients are denoted

$$\frac{1}{N} F \underline{f} = \underline{a} = (\hat{a}_0, \cdots, \hat{a}_{N-1})^T,$$

then using N-periodicity $\hat{a}_k = \hat{a}_{k-N}$ with $M = N/2$ this is

$$\frac{1}{N} F \underline{f} = \underline{a} = (\hat{a}_0, \cdots, \hat{a}_M, \hat{a}_{-M+1}, \cdots, \hat{a}_{-1})^T.$$

The operators $K_N, P_{-,N}$ are written in matrix form

$$K_N = \frac{1}{N} F^H \hat{K} F,$$

$$P_{-,N} = \frac{1}{N} F^H \hat{I}_{+,N} F,$$

where the $N \times N$ matrices are written

$$\hat{K} = diag(0, \underbrace{-i, \cdots, -i}_{M-1}, 0, \underbrace{i, \cdots, i}_{M-1}),$$

$$\hat{I}_{+,N} = diag(\underbrace{1, 1, \cdots, 1}_{M}, \underbrace{0, 0, \cdots, 0}_{M}).$$

It is noted that the evaluation of $\hat{K}$, $\hat{I}_{+,N}$ requires $O(N)$ operations and F and F^H can be computed by N-point FFT in $O(N \log N)$ operations. Thus the computational cost of K_N, $P_{-,N}$ is of order $O(N \log N)$ with two FFTs.

1.3 Fornberg's method for the simply connected case

Here Fornberg's [8] Newton-like method for the interior of the disk is presented. The following is a short analysis of [19, 23] and a discussion of the eigenvalue structure of the inner linear systems. This will be useful in the examination of the multiply connected case.

The following condition will be used; see [11, sec. 14.3.I]:

Theorem 1.4. *A function $f \in \mathrm{Lip}(C)$ on the boundary C of the unit disk extends to an analytic function in the interior of the disk with $f(0) = 0$ if and only if*

$$P_- f(e^{i\theta}) = 0. \tag{1.2}$$

The problem is to find the conformal map f from the interior of the unit disk to the interior of a smooth Jordan curve $\Gamma : \gamma(S)$ parametrized by, for instance, arclength S with $f(0) = 0$ and $f'(0) > 0$ or $f(1)$ fixed. In this case, f extends smoothly to the boundary and $f(e^{i\theta}) = \gamma(S(\theta))$. The numerical problem is to approximate the boundary correspondence $S(\theta)$. This will yield an approximation to a Taylor series by the following theorem.

Theorem 1.5. *The function $f(z)$ has the series representation $f(z) = \sum_{k=0}^{\infty} a_k z^k$.*

Proof. Let C be the boundary for the unit disk. Then for all z on the interior of the disk the Cauchy integral formula gives

$$f(z) = \frac{1}{2\pi i} \int_C \frac{f(\zeta)}{\zeta - z}\, d\zeta.$$

Note that $d\zeta = ie^{i\theta}\,d\theta$ and $\frac{|z|}{|\zeta|} < 1$, since $\zeta = e^{i\theta}$ for $0 \le \theta \le 2\pi$. Then

$$f(z) = \frac{1}{2\pi i}\int_C f(\zeta)\frac{1}{\zeta}\cdot\frac{1}{1-z/\zeta}\,d\zeta = \frac{1}{2\pi}\int_C f(\zeta)\sum_{k=0}^{\infty}\left(\frac{z}{\zeta}\right)^k\frac{d\zeta}{\zeta}$$
$$= \frac{1}{2\pi}\int_0^{2\pi} f(e^{i\theta})\sum_{k=0}^{\infty}(ze^{-i\theta})^k\,d\theta = \sum_{k=0}^{\infty} z^k\frac{1}{2\pi}\int_0^{2\pi} f(e^{i\theta})e^{-ik\theta}\,d\theta.$$

Now define the Fourier coefficients $a_k := \frac{1}{2\pi}\int_0^{2\pi} f(e^{i\theta})e^{-ik\theta}\,d\theta$, and the conclusion follows. □

A Newton-like method can be used for determining $S(\theta)$. At the kth Newton step a correction $U^{(k)}(\theta)$ real to $S^{(k)}(\theta)$ is computed from the condition that the linearization

$$f(e^{i\theta}) \approx \xi(\theta) + e^{i\beta(\theta)}U^{(k)}(\theta),$$

where $\xi(\theta) = \gamma(S^{(k)}(\theta))$ and $\beta(\theta) = \arg\gamma'(S^{(k)}(\theta))$, extends analytically to the interior of the unit disk with $f(0) = 0$.

From the analyticity condition (1.2)

$$2P_- f = (I - iK + J)f = 0.$$

This implies (with $U = U^{(k)}$) that

$$(I - iK + J)e^{i\beta(\theta)}U(\theta) = -2P_-\xi(\theta).$$

Using the fact U is real gives

$$(I + R)U = b$$

where $R = \mathrm{Re}(e^{-i\beta}(J - iK)e^{i\beta})$ and $b = -\mathrm{Re}(e^{-i\beta}(I - iK + J)\xi)$. Considering

$$\begin{aligned}
RU &= \mathrm{Re}\,(e^{-i\beta}(J - iK)(e^{i\beta}U)) = \mathrm{Re}\,(e^{-i\beta}J(e^{i\beta}U) - ie^{-i\beta}) \\
&= \mathrm{Re}\,\left(\frac{1}{2\pi}\int_0^{2\pi} e^{-i\beta(\theta)+i\beta(\phi)}U(\phi)\,d\phi - \frac{i}{2\pi}\int_0^{2\pi} e^{-i\beta(\theta)+i\beta(\phi)}\cot\left(\frac{\theta-\phi}{2}\right)U(\phi)\,d\phi\right) \\
&= \frac{1}{2\pi}\int_0^{2\pi} \cos(\beta(\phi)-\beta(\theta))U(\phi)\,d\phi + \frac{1}{2\pi}\int_0^{2\pi} \sin(\beta(\phi)-\beta(\theta))\cot\left(\frac{\theta-\phi}{2}\right)U(\phi)\,d\phi \\
&= \frac{1}{2\pi}\int_0^{2\pi} \frac{\cos(\beta(\phi)-\beta(\theta))\sin\left(\frac{\theta-\phi}{2}\right) + \sin(\beta(\phi)-\beta(\theta))\cos\left(\frac{\theta-\phi}{2}\right)}{\sin\left(\frac{\theta-\phi}{2}\right)}U(\phi)\,d\phi \\
&= \frac{1}{2\pi}\int_0^{2\pi} \frac{\sin\left(\beta(\phi)-\beta(\theta)+\frac{\theta-\phi}{2}\right)}{\sin\left(\frac{\theta-\phi}{2}\right)}U(\phi)\,d\phi,
\end{aligned}$$

define the integral operator

$$RU(\theta) := \int_0^{2\pi} R(\theta,\phi)U(\phi)\,d\phi = \frac{1}{2\pi}\int_0^{2\pi} \frac{\sin\left(\beta(\phi)-\beta(\theta)+\frac{\theta-\phi}{2}\right)}{\sin\left(\frac{\theta-\phi}{2}\right)}U(\phi)\,d\phi,$$

so consequently R can be represented as a Fredholm integral operator on $L^2(0,2\pi)$ with kernel $R(\theta,\phi)$. For γ sufficiently smooth R is a symmetric, compact operator on L^2; see [19, section 4] and [23]. With $E = \mathrm{diag}_j(e^{i\beta(\theta_j)})$, $j = 0, 1, \cdots, N-1$, discretization by N-point trigonometric interpolation gives

$$(I_N + R_N)\underline{U} = \underline{b}.$$

The matrix

$$I_N + R_N = \frac{2}{N}\mathrm{Re}(E^H F^H I_{+,N} F E) \tag{1.3}$$

is symmetric and positive (semi)definite with eigenvalues well-grouped around 1 and thus the conjugate gradient method converges superlinearly. The FFT is used to perform the matrix-vector multiplications in $O(N \log N)$. The Newton update is given by $\underline{S}^{(k+1)} = \underline{S}^{(k)} + \underline{U}^{(k)}$, with $U_0 = 0$ set to fix a boundary point as in [8]. Equation (1.3) is a slight reformulation of [8]. In [7, 8] computations which use the conjugate gradient method to solve (1.3) are reported.

1.4 The conjugate gradient method

In computing the conformal maps one must solve a linear system of the form $A\underline{u} = \underline{b}$ where A is a discretization of the identity plus a compact operator. This section is a discussion of why the iterative conjugate gradient method is useful in this case. The statements concerning compact operators are taken from [17].

Definition 1.2. *Suppose X and Y are Banach spaces and B is the open unit ball in X. A linear map $\mathcal{T} : X \to Y$ is said to be* compact *if the closure of $\mathcal{T}(B)$ is compact in Y.*

Definition 1.3. *The* spectrum *$\sigma(\mathcal{T})$ of an operator $\mathcal{T}$ on a Banach space is the set of all scalars λ such that $\mathcal{T} - \lambda I$ is not invertible. If $\mathcal{T} - \lambda I$ is not one-to-one, then λ is said to be an* eigenvalue *of $\mathcal{T}$.*

Theorem 1.6. *If $\mathcal{T}$ is a compact operator on a Banach space, then $\sigma(\mathcal{T})$ is compact, is at most countable, and has at most zero as the only limit point.*

The useful property used here is that the discretization of a compact operator results in a matrix that is numerically of low rank.

The conjugate gradient method (CG) is a well-known fast iterative solver for linear systems $Ax = b$ where A is a positive-(semi)definite matrix. The CG algorithm is exceedingly simple in implementation. Figure 1.2 shows an implementation in MATLAB with `x` as

```
x = 0; r = b; p = r;
while (norm(r) > stop_value) && (r ~= 0)
    norm_rprev = norm(r);
    alpha = norm_rprev^2/(p'*A*p);
    x = x + alpha*p;
    r = r - alpha*A*p;
    beta = norm(r)^2/norm_rprev^2;
    p = r + beta*p;
end
```

Figure 1.2: A simple CG implementation in MATLAB.

the approximate solution at each step and `r` as the residual $r = b - Ax$ at each step. There

are two properties that make CG desirable for the method presented in this thesis. The first is that the algorithm requires only one matrix-vector multiplication per iteration, which puts it on the order of $O(n^2)$. The second is indicated by [10, Theorem 10.2.4].

Theorem 1.7. *If $A = I + R$ is an $n \times n$ symmetric positive-definite matrix and the rank of R is k, then the CG algorithm converges in at most $k + 1$ steps.*

It follows that if $k << n$, as in the case presented in the subsequent, then CG will converge in relatively few iterations.

CHAPTER 2

THE GENERALIZED METHOD

2.1 The circle map problem

We state again the circle map problem. The circle domain will be defined as the m-connected region D that is interior to the boundary $C = C_1 - C_2 - \cdots - C_m$ where C_1 is the unit circle, and the mutually exterior circles $C_2, \ldots, C_m$ are on the interior C_1. None of the boundary circles intersect. The target region Ω is the m-connected region interior to a smooth boundary $\Gamma = \Gamma_1 - \Gamma_2 - \cdots - \Gamma_m$ where mutually exterior smooth curves $\Gamma_2, \ldots, \Gamma_m$ are interior to a smooth curve Γ_1. As with the circle domain the boundary curves do not intersect. The objective, given the target region in the w-plane, is to find the particular circle domain in the z-plane along with the conformal map $w = f(z)$ that produces the given image. Here normalization is done by fixing $f(1)$ and $f(z_0)$ where z_0 is any point other than $z = 1$ in the circle domain. The circle map problem is then to find the centers c_ν, and radii ρ_ν, $\nu = 2, \ldots, m$, of the $m-1$ circles C_ν in the domain, along with the boundary correspondences $S_\nu = S_\nu(\theta)$, $\nu = 1, \ldots, m$ such that

$$f(c_\nu + \rho_\nu e^{i\theta}) = \gamma_\nu(S_\nu(\theta)),$$

where the smooth target boundaries $\Gamma_\nu : \gamma_\nu(S)$ are parametrized, e.g., by arclength S.

2.2 Form of the map

A computationally convenient form of this map is easily determined in advance. Since $f(c_\nu + \rho_\nu e^{i\theta})$ is a 2π periodic function on each circle C_ν it will help to define the Fourier

coefficients for $1 \leq \nu \leq m$ and $j > 0$ by

$$a_{\nu,j} := \frac{1}{2\pi} \int_0^{2\pi} f(c_\nu + \rho_\nu e^{i\theta}) e^{-ij\theta} \, d\theta. \tag{2.4}$$

Theorem 2.1. *The map described above has the series representation*

$$f(z) = \sum_{j=0}^{\infty} a_{1,j} z^j + \sum_{\nu=2}^{m} \sum_{j=1}^{\infty} a_{\nu,-j} \left(\frac{\rho_\nu}{z - c_\nu} \right)^j. \tag{2.5}$$

Proof. For a point z in D (with z not on the boundary) the Cauchy integral formula gives

$$f(z) = \frac{1}{2\pi i} \int_C \frac{f(\zeta)}{\zeta - z} \, d\zeta = \frac{1}{2\pi i} \int_{C_1} \frac{f(\zeta)}{\zeta - z} \, d\zeta - \sum_{\nu=2}^{m} \frac{1}{2\pi i} \int_{C_\nu} \frac{f(\zeta)}{\zeta - z} \, d\zeta. \tag{2.6}$$

If $\zeta = e^{i\theta}$ for $0 \leq \theta \leq 2\pi$, then $d\zeta = ie^{i\theta} \, d\theta$ and $\frac{|z|}{|\zeta|} < 1$. Additionally if $\zeta = c_\nu + \rho_\nu e^{i\theta}$, then $\frac{|\zeta - c_\nu|}{|z - c_\nu|} < 1$ and $d\zeta = i\rho_\nu e^{i\theta} \, d\theta$. By expanding the Cauchy kernels, the integrals in (2.6) can then be written

$$\begin{aligned} \frac{1}{2\pi i} \int_{C_1} \frac{f(\zeta)}{\zeta - z} \, d\zeta &= \frac{1}{2\pi i} \int_{C_1} f(\zeta) \sum_{j=0}^{\infty} \left(\frac{z}{\zeta} \right)^j \frac{d\zeta}{\zeta} = \frac{1}{2\pi} \int_0^{2\pi} f(e^{i\theta}) \sum_{j=0}^{\infty} (ze^{-i\theta})^j \, d\theta \\ &= \sum_{j=0}^{\infty} \left[z^j \frac{1}{2\pi} \int_0^{2\pi} f(e^{i\theta}) e^{-ij\theta} \, d\theta \right] \end{aligned}$$

and, similarly for $\nu = 2, \ldots, m$,

$$\begin{aligned} \frac{1}{2\pi i} \int_{C_\nu} \frac{f(\zeta)}{\zeta - c_\nu - (z - c_\nu)} \, d\zeta &= -\frac{1}{2\pi i} \int_{C_\nu} f(\zeta) \frac{1}{z - c_\nu} \sum_{j=0}^{\infty} \left(\frac{\zeta - c_\nu}{z - c_\nu} \right)^j \, d\zeta \\ &= -\frac{1}{2\pi} \int_0^{2\pi} f(c_\nu + \rho_\nu e^{i\theta}) \frac{1}{z - c_\nu} \sum_{j=0}^{\infty} \left(\frac{\rho_\nu e^{i\theta}}{z - c_\nu} \right)^j \rho_\nu e^{i\theta} \, d\theta \\ &= -\sum_{j=1}^{\infty} \left[\left(\frac{\rho_\nu}{z - c_\nu} \right)^j \frac{1}{2\pi} \int_0^{2\pi} f(c_\nu + \rho_\nu e^{i\theta}) e^{ij\theta} \, d\theta \right]. \end{aligned}$$

□

2.3 Analyticity conditions

The conditions for analytic extension (analyticity conditions) are derived from the following theorem.

Theorem 2.2. *Let C be a positively oriented, Lipschitz continuous curve with D the region bounded by C and D^- the compliment of $D \cup C$. A function $f \in \mathrm{Lip}(C)$ can be continued analytically into D if and only if*

$$\frac{1}{2\pi}\int_C \frac{f(\zeta)}{\zeta - z}\,d\zeta = 0, \quad \forall z \in D^-.$$

Proof. This theorem can be proven immediately for a multiply connected region from the theorem for the simply connected, [11, Theorem 14.3a], by slitting the multiply connected region to form a simply connected region. This can also be found in [13, Section 24, pp.61-63]. □

The analyticity conditions given by the next theorem show how the Fourier coefficients used in the map (2.5) might be found.

Theorem 2.3. *A function $f \in \mathrm{Lip}(C)$ extends analytically into D if and only if for all $k \geq 0$*

$$a_{1,-(k+1)} - \sum_{\nu=2}^{m}\sum_{j=0}^{k}\binom{k}{j}\rho_\nu^{j+1}c_\nu^{k-j}a_{\nu,-(j+1)} = 0 \tag{2.7}$$

and

$$\sum_{j=0}^{\infty} B_{k+1,j}\rho_\ell^k c_\ell^j a_{1,k+j} - a_{\ell,k} - \sum_{\substack{\nu=2\\ \nu\neq\ell}}^{m}\sum_{j=0}^{\infty}\frac{\rho_\ell^k}{(c_\nu - c_\ell)^{k+1}}B_{k+1,j}\frac{\rho_\nu^{j+1}}{(c_\ell - c_\nu)^j}a_{\nu,-(j+1)} = 0 \tag{2.8}$$

where

$$\binom{k}{j} = \frac{k!}{j!(k-j)!} \quad \textit{and} \quad B_{k,j} = \frac{k(k+1)\cdots(k+j-1)}{j!}.$$

Proof. The proof involves applying Theorem 2.2 for z exterior to the unit disk or inside each of the interior disks, expanding the function in the appropriate Laurent series, and setting the resulting series to 0.

Outside C_1: Let z be in D_1 where $|z| > 1$. Then $\frac{|\zeta|}{|z|} < 1$ for ζ on any circle $C_1, \ldots, C_m$, and Theorem 2.2 gives

$$\frac{1}{2\pi i}\int_C \frac{f(\zeta)}{\zeta - z}\,d\zeta = -\frac{1}{2\pi i}\int_C f(\zeta)\frac{1}{z}\sum_{k=0}^{\infty}\left(\frac{\zeta}{z}\right)^k d\zeta = 0$$

or

$$-\sum_{k=0}^{\infty} z^{-k-1}\frac{1}{2\pi i}\int_C f(\zeta)\zeta^k\,d\zeta = 0. \tag{2.9}$$

Equivalently the integral in (2.9) must be zero for all $k \geq 0$, that is

$$\begin{aligned}
0 &= \frac{1}{2\pi i}\int_C f(\zeta)\zeta^k\,d\zeta = \frac{1}{2\pi i}\int_{C_1} f(\zeta)\zeta^k\,d\zeta - \sum_{\nu=2}^{m}\frac{1}{2\pi i}\int_{C_\nu} f(\zeta)\zeta^k\,d\zeta \\
&= \frac{1}{2\pi}\int_0^{2\pi} f(e^{i\theta})e^{i(k+1)\theta}\,d\theta - \sum_{\nu=2}^{m}\frac{1}{2\pi}\int_0^{2\pi} f(c_\nu+\rho_\nu e^{i\theta})(c_\nu+\rho_\nu e^{i\theta})^k\rho_\nu e^{i\theta}\,d\theta \\
&= \frac{1}{2\pi}\int_0^{2\pi} f(e^{i\theta})e^{i(k+1)\theta}\,d\theta - \sum_{\nu=2}^{m}\frac{1}{2\pi}\int_0^{2\pi} f(c_\nu+\rho_\nu e^{i\theta})\left(\sum_{j=0}^{k}\binom{k}{j}c_\nu^{k-j}\rho_\nu^j e^{ij\theta}\right)\rho_\nu e^{i\theta}\,d\theta \\
&= \frac{1}{2\pi}\int_0^{2\pi} f(e^{i\theta})e^{i(k+1)\theta}\,d\theta - \sum_{\nu=2}^{m}\sum_{j=0}^{k}\binom{k}{j}\rho_\nu^{j+1}c_\nu^{k-j}\frac{1}{2\pi}\int_0^{2\pi} f(c_\nu+\rho_\nu e^{i\theta})e^{i(j+1)\theta}\,d\theta
\end{aligned} \tag{2.10}$$

Using the definition given in (2.4) for Fourier coefficients, the result is now the first analyticity condition

$$a_{1,-(k+1)} - \sum_{\nu=2}^{m}\sum_{j=0}^{k}\binom{k}{j}\rho_\nu^{j+1}c_\nu^{k-j}a_{\nu,-(j+1)} = 0.$$

Inside C_ℓ ($2 \leq \ell \leq m$): Consider now the case where z is in the interior of one of the disks D_ℓ. Then $\frac{|z-c_\ell|}{|\zeta-c_\ell|} < 1$ for ζ on any $C_1,\ldots,C_m$, and

$$0 = \frac{1}{2\pi i}\int_C \frac{f(\zeta)}{\zeta - z}\,d\zeta = \frac{1}{2\pi i}\int_C \frac{f(\zeta)}{\zeta - c_\ell - (z-c_\ell)}\,d\zeta = \frac{1}{2\pi i}\int_C f(\zeta)\frac{1}{\zeta-c_\ell}\sum_{k=0}^{\infty}\left(\frac{z-c_\ell}{\zeta-c_\ell}\right)^k d\zeta$$

or

$$0 = \sum_{k=0}^{\infty}(z-c_\ell)^k\frac{1}{2\pi i}\int_C f(\zeta)(\zeta-c_\ell)^{-k-1}\,d\zeta. \tag{2.11}$$

Again the integral in (2.11) must be zero for all $k \geq 0$. The resulting analyticity condition is best understood if the integral is examined on each $C_1,\ldots,C_m$ in turn, starting with C_1. But first note that

$$\frac{1}{(1-z)^k} = \sum_{j=0}^{\infty} B_{k,j}z^j$$

for positive integers $k > 0$, and $|z| < 1$. Since $\frac{|c_\ell|}{|e^{i\theta}|} < 1$, one can write

$$(e^{i\theta}-c_\ell)^{-k-1} = \frac{1}{e^{i(k+1)\theta}}\cdot\frac{1}{\left(1-\frac{c_\ell}{e^{i\theta}}\right)^{k+1}} = \frac{1}{e^{i(k+1)\theta}}\sum_{j=0}^{\infty}B_{k+1,j}\left(\frac{c_\ell}{e^{i\theta}}\right)^j,$$

and so

$$\begin{aligned}\frac{1}{2\pi i}\int_{C_1} f(\zeta)(\zeta-c_\ell)^{-k-1}\,d\zeta &= \frac{1}{2\pi}\int_0^{2\pi} f(e^{i\theta})(e^{i\theta}-c_\ell)^{-k-1}e^{i\theta}\,d\theta \\ &= \sum_{j=0}^{\infty} B_{k+1,j}c_\ell^j \frac{1}{2\pi}\int_0^{2\pi} f(e^{i\theta})e^{-i(k+j)\theta}\,d\theta.\end{aligned} \tag{2.12}$$

Since $\rho_\nu < |c_\ell - c_\nu|$ for C_ν, $2 \le \nu \le m$ and $\nu \neq \ell$, one has

$$\begin{aligned}(\rho_\nu e^{i\theta} - (c_\ell - c_\nu))^{-k-1} &= \frac{1}{(c_\ell - c_\nu)^{k+1}(-1)^{k+1}\left(1-\frac{\rho_\nu e^{i\theta}}{c_\ell - c_\nu}\right)^{k+1}} \\ &= \frac{1}{(c_\nu - c_\ell)^{k+1}}\sum_{j=0}^{\infty} B_{k+1,j}\left(\frac{\rho_\nu e^{i\theta}}{c_\ell - c_\nu}\right)^j,\end{aligned}$$

thus

$$\begin{aligned}\frac{1}{2\pi i}\int_{C_\nu} f(\zeta)(\zeta-c_\ell)^{-k-1}\,d\zeta &= \frac{1}{2\pi}\int_0^{2\pi} f(c_\nu+\rho_\nu e^{i\theta})(\rho_\nu e^{i\theta}-(c_\ell-c_\nu))^{-k-1}\rho_\nu e^{i\theta}\,d\theta \\ &= \frac{1}{2\pi}\int_0^{2\pi} f(c_\nu+\rho_\nu e^{i\theta})\frac{1}{(c_\nu-c_\ell)^{k+1}}\sum_{j=0}^{\infty} B_{k+1,j}\left(\frac{\rho_\nu e^{i\theta}}{c_\ell-c_\nu}\right)^j \rho_\nu e^{i\theta}\,d\theta \\ &= \frac{1}{(c_\nu-c_\ell)^{k+1}}\sum_{j=0}^{\infty} B_{k+1,j}\frac{\rho_\nu^{j+1}}{(c_\ell-c_\nu)^j}\cdot\frac{1}{2\pi}\int_0^{2\pi} f(c_\nu+\rho_\nu e^{i\theta})e^{i(j+1)\theta}\,d\theta.\end{aligned} \tag{2.13}$$

And finally around C_ℓ

$$\begin{aligned}\frac{1}{2\pi i}\int_{C_\ell} f(\zeta)(\zeta-c_\ell)^{-k-1}\,d\zeta &= \frac{1}{2\pi}\int_0^{2\pi} f(c_\ell+\rho_\ell e^{i\theta})\rho_\ell^{-k-1}e^{-i(k+1)\theta}\rho_\ell e^{i\theta}\,d\theta \\ &= \frac{1}{2\pi}\int_0^{2\pi} f(c_\ell+\rho_\ell e^{i\theta})\rho_\ell^{-k}e^{-ik\theta}\,d\theta.\end{aligned} \tag{2.14}$$

Using equations (2.12), (2.13), and (2.14) allows rewriting the integral

$$\frac{1}{2\pi i}\int_C f(\zeta)(\zeta-c_\ell)^{-k-1}\,d\zeta = 0$$

from (2.11) as the condition

$$\sum_{j=0}^{\infty} B_{k+1,j}\rho_\ell^k c_\ell^j a_{1,k+j} - a_{\ell,k} - \sum_{\substack{\nu=2\\ \nu\neq\ell}}^{m}\sum_{j=0}^{\infty}\frac{\rho_\ell^k}{(c_\nu-c_\ell)^{k+1}}B_{k+1,j}\frac{\rho_\nu^{j+1}}{(c_\ell-c_\nu)^j}a_{\nu,-(j+1)} = 0.$$

□

Left outstanding is the issue of discovering the correct values for ρ_ν and c_ν, but this should be clarified in the subsequent sections.

2.4 Linearization

A Newton-like method is applied to find the boundary correspondences $S_\nu = S_\nu(\theta)$ along with the centers $c_2, \ldots, c_m$ and the radii $\rho_2, \ldots, \rho_m$ of the domain circles such that $f(c_\nu + \rho_\nu e^{i\theta}) = \gamma_\nu(S_\nu(\theta))$ for $1 \leq \nu \leq m$. At each step of the Newton iteration a 2π periodic update $U_\nu(\theta)$ to $S_\nu(\theta)$ must be calculated, as well as the updates δc_ν for the centers and $\delta\rho_\nu$ for the radii. This is accomplished by first writing the approximations

$$\gamma_\nu(S_\nu(\theta) + U_\nu(\theta)) \approx \gamma_\nu(S_\nu(\theta)) + \gamma_\nu'(S_\nu(\theta))U_\nu(\theta) \tag{2.15}$$

and

$$\begin{aligned}(f + \delta f)(c_\nu + \delta c_\nu + (\rho_\nu + \delta\rho_\nu)e^{i\theta}) \\ \approx (f + \delta f)(c_\nu + \delta c_\nu) + f'(c_\nu + \rho_\nu e^{i\theta})(\delta c_\nu + \delta\rho_\nu e^{i\theta}).\end{aligned} \tag{2.16}$$

Equating the approximations (2.15) and (2.16) allows writing

$$\begin{aligned}(f + \delta f)(c_\nu + \rho_\nu e^{i\theta}) \\ = \gamma_\nu(S_\nu(\theta)) + \gamma_\nu'(S_\nu(\theta))U_\nu(\theta) - f'(c_\nu + \rho_\nu e^{i\theta})(\delta c_\nu + \delta\rho_\nu e^{i\theta}).\end{aligned} \tag{2.17}$$

Define for convenience

$$\begin{aligned}\xi_\nu(\theta) &:= \gamma_\nu(S_\nu(\theta)), \\ \eta_\nu(\theta) &:= \gamma_\nu'(S_\nu(\theta)), \text{ and} \\ \zeta_\nu(\theta) &:= -f'(c_\nu + \rho_\nu e^{i\theta})e^{i\theta} = i\rho_\nu^{-1}\eta_\nu S_\nu'(\theta),\end{aligned}$$

and thus (2.17) can be written as the linear conditions

$$(f + \delta f)(e^{i\theta}) = \xi_1(\theta) + \eta_1(\theta)U_1(\theta) \tag{2.18}$$

and

$$(f + \delta f)(c_\nu + \rho_\nu e^{i\theta}) = \xi_\nu(\theta) + \eta_\nu(\theta)U_\nu(\theta) + \zeta_\nu(\theta)(\delta\rho_\nu + \delta c_\nu e^{-i\theta}). \tag{2.19}$$

A linear system, subsequently defined, is solved to find the corrections $U_1(\theta)$, $U_\nu(\theta)$, δc_ν, and $\delta\rho_\nu$; and the updates at each step n of the Newton iteration are then

$$\begin{aligned} S_\nu^{(n)}(\theta) &= S_\nu^{(n-1)}(\theta) + U_\nu^{(n-1)}(\theta), \quad \nu = 1, \ldots, m \\ c_\nu^{(n)} &= c_\nu^{(n-1)} + \delta c_\nu^{(n-1)}, \quad \nu = 2, \ldots, m \\ \rho_\nu^{(n)} &= \rho_\nu^{(n-1)} + \delta \rho_\nu^{(n-1)}, \quad \nu = 2, \ldots, m. \end{aligned} \tag{2.20}$$

This linearization was introduced in [3, 6], and justified in [21].

Like other Newton methods a reasonable initial guess is required for each S_ν, c_ν, and ρ_ν. Experimentation has shown that the "reasonability" of an initial guess appears to depend on the target region under consideration, but it is not yet clear exactly what factors are at play in this determination.

2.5 Normalization conditions

Normalization is done by specifying three real conditions for the map. One condition is given by fixing the boundary correspondence $f(1) = \gamma_1(0)$. This is accomplished by forcing the update for the boundary component $S_1(0)$ to be zero at every iteration. Fixing one other interior point in the map, $f(z_0) = w_0$, takes care of the remaining two real conditions. The computationally convenient (2.5) yields in this case

$$w_0 = f(z_0) = \sum_{k=0}^{\infty} a_{1,k} z_0^k + \sum_{\nu=2}^{m} \sum_{k=1}^{\infty} a_{\nu,-k} \left(\frac{\rho_\nu}{z_0 - c_\nu} \right)^k. \tag{2.21}$$

2.6 Discretization and matrix formation

Discretization is done using N-point trigonometric interpolation. Let $a_{1,k}, \ldots, a_{m,k}$ now denote the discrete Fourier coefficients. With $N = 2M$ and the N-periodicity of the discrete coefficients, $a_{\nu,k} = a_{\nu,k+N}$, note that

$$\underline{a}_\nu = (a_{\nu,0}, a_{\nu,1}, \ldots, a_{\nu,N-1})^T = (a_{\nu,0}, \ldots, a_{\nu,M-1}, a_{\nu,-M}, \ldots, a_{\nu,-1})^T$$

for $1 \leq \nu \leq m$. If the analyticity and normalization conditions are limited to M terms and the analyticity conditions are limited to M equations (by making $k = 0, \ldots, M-1$ or $k = 1, \ldots, M$), then the discrete form of equations (2.7), (2.8), and (2.21) become

$$a_{1,-(k+1)} - \sum_{\nu=2}^{m} \sum_{j=0}^{k} \binom{k}{j} \rho_\nu^{j+1} c_\nu^{k-j} a_{\nu,-(j+1)} = 0, \tag{2.22}$$

$$\sum_{j=0}^{M-1} B_{k+1,j} \rho_\ell^k c_\ell^j a_{1,k+j} - a_{\ell,k} - \sum_{\substack{\nu=2 \\ \nu \neq \ell}}^{m} \sum_{j=0}^{M-1} \frac{\rho_\ell^k}{(c_\nu - c_\ell)^{k+1}} B_{k+1,j} \frac{\rho_\nu^{j+1}}{(c_\ell - c_\nu)^j} a_{\nu,-(j+1)} = 0, \tag{2.23}$$

and

$$w_0 = f(z_0) = \sum_{j=0}^{M-1} a_{1,j} z_0^j + \sum_{\nu=2}^{m} \sum_{j=1}^{M} a_{\nu,-j} \left(\frac{\rho_\nu}{z_0 - c_\nu} \right)^j. \tag{2.24}$$

This system of linear equations (2.22), (2.23), and (2.24) can be written in matrix form

$$P\underline{a} = P_1 \underline{a}_1 + \cdots + P_m \underline{a}_m = [P_1 \quad \cdots \quad P_m] \begin{bmatrix} \underline{a}_1 \\ \vdots \\ \underline{a}_m \end{bmatrix} = \begin{bmatrix} 0 \\ \vdots \\ 0 \\ w_0 \end{bmatrix} := \underline{r}, \tag{2.25}$$

with $\underline{r}$ by definition as an $mM + 1$ column vector. The matrices P_1 and P_ν, $\nu = 2, \ldots, m$, have the block structure

$$P_1 = \begin{bmatrix} 0 & I \\ P_{2,1} & 0 \\ \vdots & \vdots \\ P_{m,1} & 0 \\ p_1 & 0 \end{bmatrix} \quad \text{and} \quad \underset{2 \leq \nu \leq m}{P_\nu} = \begin{bmatrix} 0 & -P_{1,\nu} \\ \vdots & \vdots \\ 0 & -P_{\nu-1,\nu} \\ -I & 0 \\ 0 & -P_{\nu+1,\nu} \\ \vdots & \vdots \\ 0 & -P_{m,\nu} \\ 0 & -p_\nu \end{bmatrix} \tag{2.26}$$

where each submatrix is $M \times M$ with the exception of the p submatrices which are $1 \times M$. The non-identity submatrices on the first block-row of P_ν and all of the submatrices of P_1

are upper-triangular. The remaining submatrices are dense and have a computational cost of $O(n^2)$ to form. For the details of these submatrices see Appendix A.

The linearization conditions (2.18) and (2.19) written as vectors, with

$$\underline{\theta} := \frac{2\pi}{N}(0, 1, \ldots, N-1)^T \quad \text{and} \quad \underline{\xi}_{\nu} := \xi_{\nu}(\underline{\theta}), \quad \text{etc.},$$

take the form

$$N\underline{a}_1 = F\underline{\xi}_1 + FE_1\underline{U}_1 \tag{2.27}$$

$$N\underline{a}_{\nu} = F\underline{\xi}_{\nu} + FE_{\nu}\underline{U}_{\nu} + \delta\rho_{\nu}F\underline{\zeta}_{\nu} + \delta c_{\nu}F(\underline{q} * \underline{\zeta}_{\nu}) \tag{2.28}$$

where F is the discrete Fourier transform matrix, $E_{\nu} := \mathrm{diag}(\underline{\eta}_{\nu})$, the vector $\underline{q}$ is defined to be $\underline{q} := e^{-i\underline{\theta}}$, and $*$ denotes the Hadamard product.

For convenience the rest of this section will be presented with $m = 3$. Modification of the following for any other m is straightforward.

Combining the Newton linearization conditions (2.27) and (2.28) with the linear system (2.25) gives

$$\begin{aligned} &P_1FE_1\underline{U}_1 + P_2(FE_2\underline{U}_2 + \delta\rho_2F\underline{\zeta}_2 + (\mathrm{Re}\,\delta c_2 + i\mathrm{Im}\,\delta c_2)F(\underline{q} * \underline{\zeta}_2)) \\ &+ P_3(FE_2\underline{U}_3 + \delta\rho_3F\underline{\zeta}_3 + (\mathrm{Re}\,\delta c_3 + i\mathrm{Im}\,\delta c_3)F(\underline{q} * \underline{\zeta}_3)) = N\underline{r} - P_1F\underline{\xi}_1 - P_2F\underline{\xi}_2 - P_3F\underline{\xi}_3 := \underline{\tilde{g}}. \end{aligned}$$

Let $P = \begin{bmatrix} P_1 & P_2 & P_3 \end{bmatrix}$, and $W = \begin{bmatrix} \underline{w}_2 & \underline{w}_3 & \underline{wq}_2 & i\underline{wq}_2 & \underline{wq}_3 & i\underline{wq}_3 \end{bmatrix}$ where $\underline{w}_{\nu} := P_{\nu}F\underline{\zeta}_{\nu}$ and $\underline{wq}_{\nu} := P_{\nu}F(\underline{q} * \underline{\zeta}_{\nu})$. Given the $(3N+6) \times 1$ vector[1]

$$\underline{U} = \begin{bmatrix} \underline{U}_1^T & \underline{U}_2^T & \underline{U}_3^T & \delta\rho_2 & \delta\rho_3 & \mathrm{Re}\,\delta c_2 & \mathrm{Im}\,\delta c_2 & \mathrm{Re}\,\delta c_3 & \mathrm{Im}\,\delta c_3 \end{bmatrix}^T,$$

[1] In general the vector $\underline{U}$ will have the dimension $(mN + 3(m-1))$ for $m \geq 3$.

the linear system can now be written

$$\tilde{D}\underline{U} := \begin{bmatrix} P_1 & P_2 & P_3 & W \end{bmatrix} \begin{bmatrix} F & 0 & 0 & 0 \\ 0 & F & 0 & 0 \\ 0 & 0 & F & 0 \\ 0 & 0 & 0 & I \end{bmatrix} \begin{bmatrix} E_1 & 0 & 0 & 0 \\ 0 & E_2 & 0 & 0 \\ 0 & 0 & E_3 & 0 \\ 0 & 0 & 0 & I \end{bmatrix} \underline{U} = \underline{\tilde{g}}.$$

Defining the $1 \times (3N+6)$ vector $\underline{v}^T := (1, 0, \ldots, 0)$ allows the addition of a row to the system to force $U_1(0) = 0$ at every iteration in order to satisfy the normalized $f(1) = \gamma_1(0)$, that is

$$D := \begin{bmatrix} \tilde{D} \\ \frac{\sqrt{N}}{2}\underline{v}^T \end{bmatrix} \quad \text{and} \quad \underline{g} := \begin{bmatrix} \underline{\tilde{g}} \\ 0 \end{bmatrix}.$$

Forming the "normal equations" and using the fact $\underline{U}$ is real, we arrive at the inner linear system for $\underline{U}$,

$$A\underline{U} := \frac{2}{N}\mathrm{Re}\,(D^H D)\underline{U} = \frac{2}{N}\mathrm{Re}\,(D^H \underline{g}) := \underline{b} \tag{2.29}$$

The factor $2/N$ is added to ensure the eigenvalues cluster around 1, and not $N/2$, which facilitates the analysis below. The conjugate gradient method is now used to solve this system for $\underline{U}$, the Newton updates described in (2.20) would be applied, and we iterate until $\underline{U}$ is sufficiently small. See Appendix B details of the algorithm.

2.7 Analysis of the linear system

Consider the matrix A in (2.29),

$$A = \frac{2}{N}\mathrm{Re}\,(D^H D) = \begin{bmatrix} A_{11} & A_{12} & A_{13} & X_1 \\ A_{21} & A_{22} & A_{23} & X_2 \\ A_{31} & A_{32} & A_{33} & X_3 \\ X_1^T & X_2^T & X_3^T & W^H W \end{bmatrix} + \frac{1}{2}\underline{v}\underline{v}^T,$$

where $A_{kj} := (2/N)\mathrm{Re}\,(E_k^H F^H P_k^H P_j F E_j)$ and $X_k := (2/N)\mathrm{Re}\,(E_k^H F^H P_k^H W)$. To understand the eigenvalue distribution of A it suffices to examine the submatrix

$$\hat{A} = \begin{bmatrix} A_{11} & A_{12} & A_{13} \\ A_{21} & A_{22} & A_{23} \\ A_{31} & A_{32} & A_{33} \end{bmatrix},$$

since the eigenvalues of $\hat{A}$ and $A - \frac{1}{2}\underline{v}\underline{v}^T$ will interlace, as discussed in [10, chapter 8]. By (2.25) and (2.26)

$$P = \begin{bmatrix} P_1 & P_2 & P_3 \end{bmatrix} = \begin{bmatrix} 0 & I & 0 & -P_{12} & 0 & -P_{13} \\ P_{21} & 0 & -I & 0 & 0 & -P_{23} \\ P_{31} & 0 & 0 & -P_{32} & -I & 0 \end{bmatrix}.$$

(Note the commas in the subscripts for the submatrices as in (2.26) have been dropped for brevity.) This implies

$$P^H P = \begin{bmatrix} P_1^H P_1 & P_1^H P_2 & P_1^H P_3 \\ P_2^H P_1 & P_2^H P_2 & P_2^H P_3 \\ P_3^H P_1 & P_3^H P_2 & P_3^H P_3 \end{bmatrix},$$

and the submatrix $P_1^H P_1$ is then

$$P_1^H P_1 = \begin{bmatrix} P_{21}^H P_{21} + P_{31}^H P_{31} & 0 \\ 0 & I \end{bmatrix} = \begin{bmatrix} P_{21}^H P_{21} + P_{31}^H P_{31} & 0 \\ 0 & 0 \end{bmatrix} + \begin{bmatrix} 0 & 0 \\ 0 & I \end{bmatrix} := \Lambda_1 + I_-.$$

Rewriting A_{11},

$$A_{11} = A_{11}^{(1)} + A_{11}^{(2)} := (2/N)\mathrm{Re}\,(E_1^H F^H \Lambda_1 F E_1) + (2/N)\mathrm{Re}\,(E_1^H F^H I_- F E_1).$$

Following [3, 7, 19], it can be shown that $A_{11}^{(1)}$ as well as the off-diagonal submatrices A_{kj}, $k \neq j$, are discretizations of a compact operator. Again following [3, 7] it can be shown that $A_{11}^{(2)}$ is a discretization of $\mathrm{Re}\,(e^{-i\beta}(I + iK + J)e^{i\beta}) = I + R$ where R is the compact Fredholm integral operator discussed in section 1.2. A similar analysis applies to A_{22} and A_{33}. The upshot is that $\hat{A}$ is the discretization of the identity plus a compact operator. Since this is

effectively a low-rank perturbation of the identity the eigenvalues cluster around 1, and the conjugate gradient method applied to (2.29) works well. Figure (2.3) shows an example of this grouping of the eigenvalues.

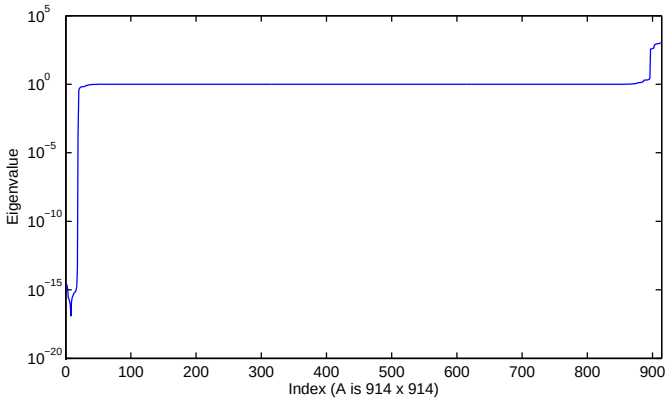

Figure 2.3: Eigenvalues of A grouped around 1 for $m = 7$ and $N = 128$.

2.8 Numerical examples

Example 2.1. As a simple test case the first example is an identity map, $m = 4$ and $N = 128$, shown in Figure 2.4. The circle domain has centers $c_2 = -0.5$, $c_3 = 0.25 + 0.43i$, and $c_4 = 0.25 - 0.43i$, each inner circle has a radius of 0.25. When given an initial guess of the exact centers and radii the algorithm converges in one step with a Newton update of order 10^{-16}. In addition the Fourier coefficients in equation (2.5) are as expected for an identity map, that is $a_{1,1} = 1$, $a_{2,1} = -0.5$, $a_{3,1} = 0.25 + 0.43i$, $a_{4,1} = 0.25 - 0.43i$, and $a_{\nu,j} = 0$ for all $j \neq 1$. On perturbation of the initial guess for the centers, set $c_2 = -.4$, $c_3 = .35 + .43i$, and $c_2 = .35 - .43i$, the algorithm converges on average in 5 iterations with the magnitude of the accuracy shown in Table 2.1; accuracy is averaged over centers and radii.

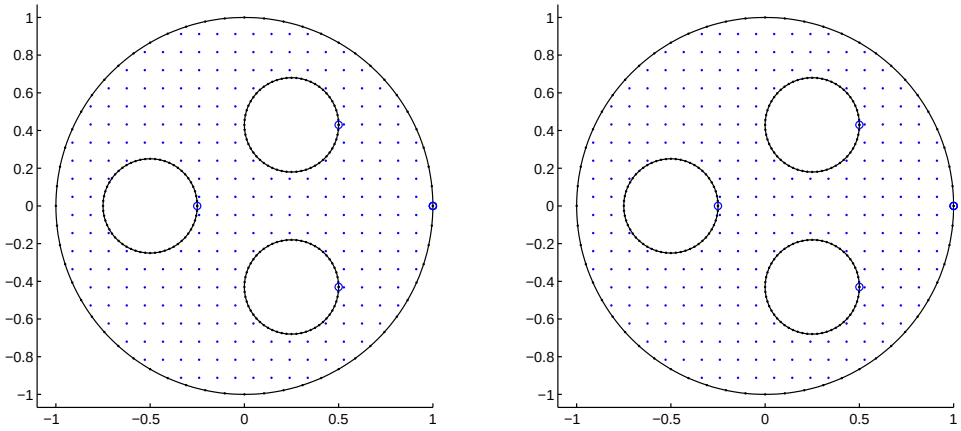

Figure 2.4: An identity map (Example 2.1), $N = 128$.

	Accuracy	
N	centers	radii
32	10^{-11}	10^{-11}
64	10^{-14}	10^{-16}
128	10^{-15}	10^{-16}
256	10^{-16}	10^{-16}

Table 2.1: Identity map accuracy.

Example 2.2. A simple ellipse region (Figure 2.5) with $m = 3$ elliptical boundaries is used to exhibit the convergence of the Newton iteration. The measure used for the Newton iteration is the infinity norm of the difference of the vectors U between iterations. These values are given in Table 2.2. The algorithm is by default set to stop when this difference has a magnitude smaller than 10^{-14}. Experimentation has shown that these updates in general will not reach an order smaller than 10^{-15}; the observed exception having been shown in the identity example.

Example 2.3. The next example (Figure 2.6) uses an inverted ellipse as an outer boundary with $m = 4$. Although as seen in the previous example the difference in successive updates

Iteration	$\|U^{(n)}\|_\infty$	# CG iter	CG residual
1	7.37×10^{-1}	20	7.34×10^{-4}
2	1.51×10^{-1}	20	8.56×10^{-4}
3	3.70×10^{-2}	19	4.10×10^{-5}
4	4.40×10^{-3}	19	4.40×10^{-6}
5	3.02×10^{-5}	18	2.87×10^{-8}
6	1.18×10^{-8}	19	7.69×10^{-12}
7	3.91×10^{-11}	16	6.74×10^{-14}
8	3.02×10^{-13}	13	6.58×10^{-16}
9	2.14×10^{-15}	8	1.65×10^{-16}

Table 2.2: Convergence of the Newton iteration for Figure 2.5, $N = 256$.

can go quickly to the limit set for the algorithm, this is not always the case. For this map after 20 iterations the algorithm was only able to gain a difference in updates of magnitude 10^{-5} with $N = 128$. It is suspected but not proven that the combination of the "pinching" by the inverted ellipse and the relative proximity of one of the inner boundaries to the outer

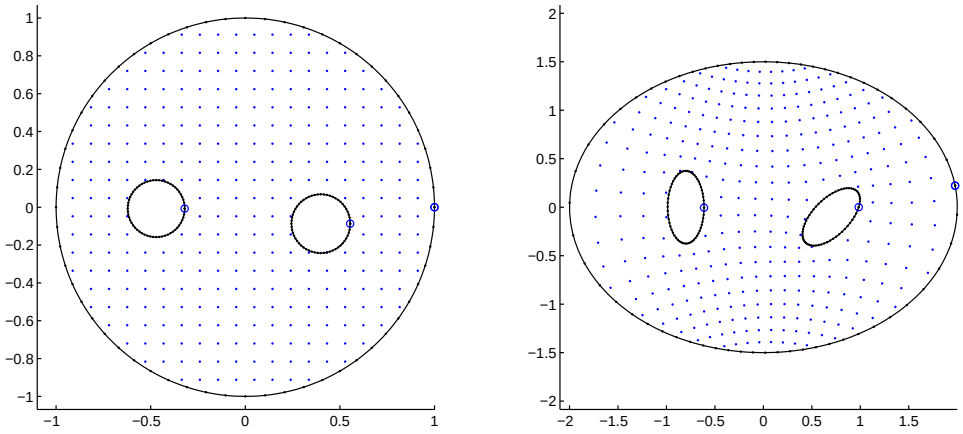

Figure 2.5: A simple ellipse target region, $N = 256$ (Example 2.2).

boundary may be the reason for this. Setting $N = 256$ gives a last Newton update of magnitude 10^{-8}, and in general adding more interpolation points should improve convergence.

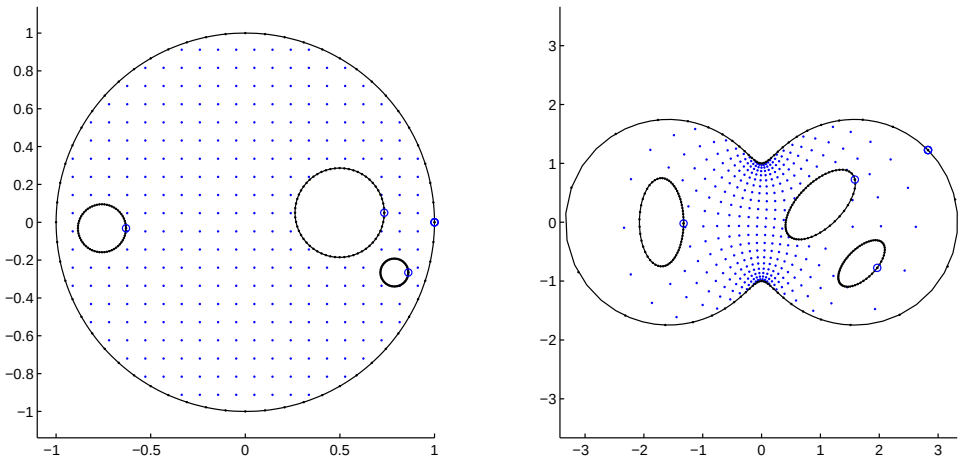

Figure 2.6: Inverted ellipse, $N = 128$ (Example 2.3).

Example 2.4. The map shown in Figure 2.7, $m = 3$ and $N = 256$, has a spline parametrized by chordal arclength as an outer boundary (the other boundary types shown in this section are parametrized by angle). This map also converged slowly; reaching a magnitude in update differences of only 10^{-8} after 20 iterations. The matrix A had 6 eigenvalues less than $\varepsilon_{\text{mach}}$ at each iteration. Plots of the eigenvalues of the submatrices of $\hat{A}$ are shown in Figure 2.8; note that on the diagonal the matrices show characteristics of being a discretization of a compact operator plus the identity while the eigenvalues of the off-diagonal entries converge to zero as should happen with discretizations of compact operators.

Example 2.5. Shown in Figure 2.9, $m = 7$, the last example is the map used to produce the eigenvalue plot shown in Figure 2.3. The eigenvalue plot was taken from the matrix A on the first Newton iteration. For $N = 128$ the last Newton iteration (20) had an update on the order of 10^{-7}, while for $N = 256$ the last update was 10^{-8}.

In the development and testing of the code for this thesis it was noticed that the matrix A has what appears to be a finite dimensional nullspace. Table 2.3 shows the numbers of zero

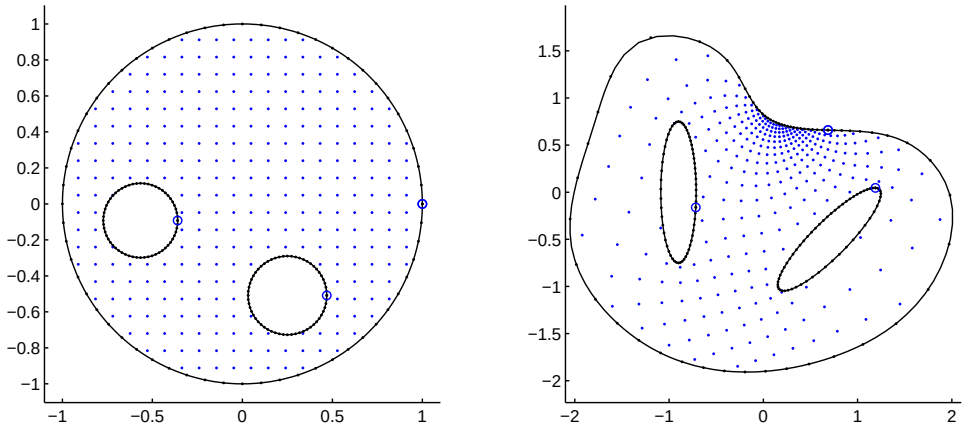

Figure 2.7: Spline outer boundary, $N = 256$ (Example 2.4).

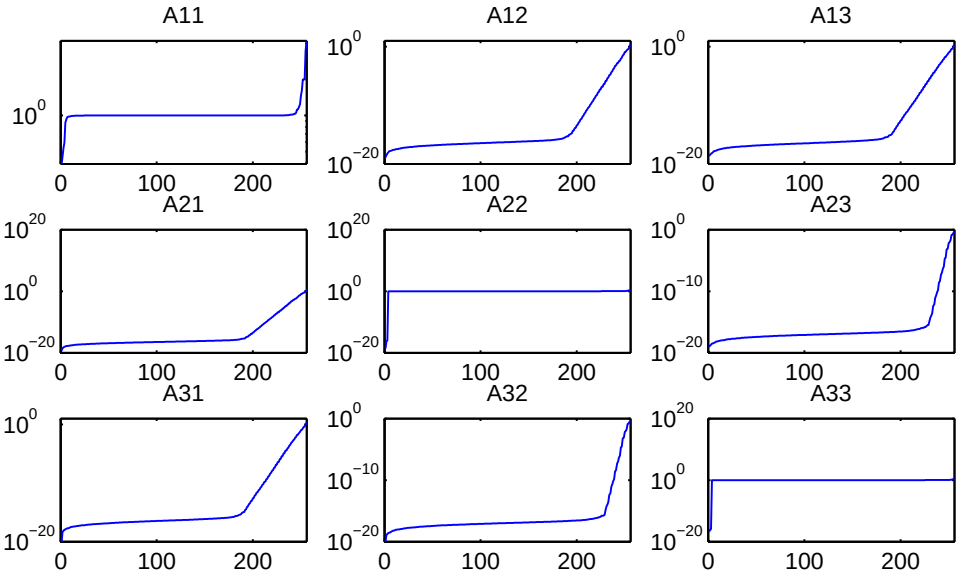

Figure 2.8: Eigenvalue plots of the submatrices of the map shown in Figure 2.7.

eigenvalues, denoted by λ_i. Note that for example 2.5 a range of values is listed. This comes from differing counts of eigenvalues less than $\varepsilon_{\text{mach}}$ at each iteration. The other examples had stable counts between iterations. These eigenvalues were not actually zero in MATLAB, but in general were close to machine epsilon, $\varepsilon_{\text{mach}}$. Code development for the numerical examples presented here was done in MATLAB on a 32-bit Intel platform, that is $\varepsilon_{\text{mach}}$ is

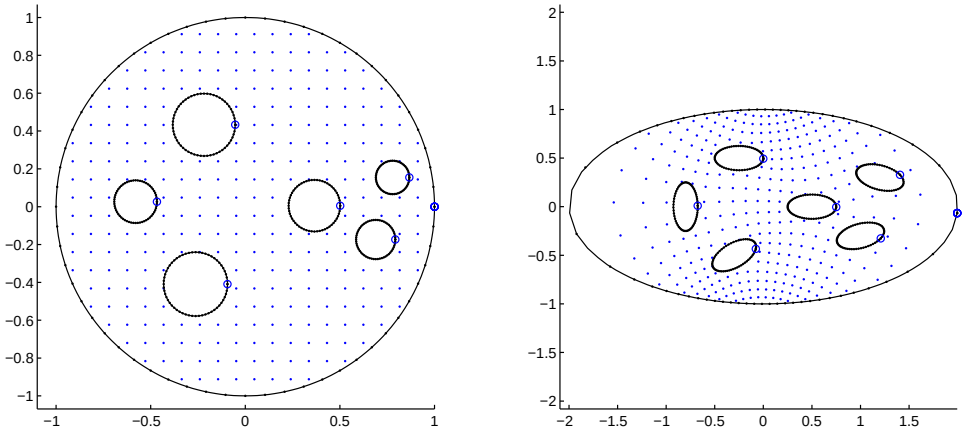

Figure 2.9: Connectivity $m = 7$, $N = 128$ (Example 2.5).

Example	m	N	$\lambda_i < \varepsilon_{\text{mach}}$	$\lambda_i < 10\varepsilon_{\text{mach}}$
1	4	128	9	9
2	3	256	6	6
3	4	128	9	9
4	3	256	6	6
5	6	128	12-15	15
5	7	128	14-17	18
5	8	128	16-19	21

Table 2.3: Number of zero eigenvalues in the numeric examples.

defined to be approximately 10^{-16}. The cause of this nullspace is undetermined at this time. An analysis of this will be part of future work.

CHAPTER 3

THE ANNULUS WITH CIRCULAR HOLES CASE

3.1 The circle map problem revisited

The setup for this problem is basically that of section 2.1 with a few minor modifications, mainly in regard to the normalization conditions. In this case the center of C_2 is fixed at the origin, $c_2 = 0$, and for $m \geq 3$ the imaginary part of the center of C_3 is set to zero. The objective remains as the computation of a conformal map $w = f(z)$ from the circle domain to the given target region.

The purpose is to see if this formulation has any theoretical or computational advantage over the general case. Clearly the number of conformal moduli is just 1 when $m = 2$ and $3(m-2)$ when $m \geq 3$; in this case the geometric meaning of the conformal moduli is clear. If $m = 2$, then ρ_2 is the only modulus. If $m = 3$, then ρ_2, ρ_3, and $\mathrm{Re}\,(c_3)$ are the moduli. For each $m > 3$ we add ρ_ν, $\mathrm{Re}\,(c_\nu)$, and $\mathrm{Im}\,(c_\nu)$, where $3 < \nu < m$, to the list of moduli.

3.2 Form of the map

Theorem 3.1. *Then the map described above has the series representation*

$$f(z) = \sum_{j=0}^{\infty} a_{1,j} z^j + \sum_{j=1}^{\infty} a_{2,-j} \left(\frac{\rho_2}{z}\right)^j + \sum_{\nu=3}^{m} \sum_{j=1}^{\infty} a_{\nu,-j} \left(\frac{\rho_\nu}{z - c_\nu}\right)^j . \tag{3.30}$$

Proof. The derivation is the same as that given for the general case in Theorem 2.1, with $c_2 = 0$. □

3.3 Analyticity conditions

Theorem 3.2. *Let D be the region on the interior of the circle C_1 and exterior to the circles $C_2, \ldots, C_m$, and suppose $f \in \mathrm{Lip}(C)$. Then f extends analytically into D if and only if for all $k \geq 0$*

$$a_{1,-(k+1)} - \rho_2^{k+1} a_{2,-(k+1)} - \sum_{\nu=3}^{m} \sum_{j=0}^{k} \binom{k}{j} \rho_\nu^{j+1} c_\nu^{k-j} a_{\nu,-(j+1)} = 0, \tag{3.31}$$

$$\rho_2^k a_{1,k} - a_{2,k} - \sum_{\nu=3}^{m} \sum_{j=0}^{\infty} \frac{\rho_2^k}{c_\nu^{k+1}} B_{k+1,j} \frac{\rho_\nu^{j+1}}{(-c_\nu)^j} a_{\nu,-(j+1)} = 0, \tag{3.32}$$

and

$$\sum_{j=0}^{\infty} \rho_\ell^k B_{k+1,j} c_\ell^j a_{1,k+j} - a_{\ell,k} - \sum_{\substack{\nu=2 \\ \nu \neq \ell}}^{m} \sum_{j=0}^{\infty} \frac{\rho_\ell^k}{(c_\nu - c_\ell)^{k+1}} B_{k+1,j} \frac{\rho_\nu^{j+1}}{(c_\ell - c_\nu)^j} a_{\nu,-(j+1)} = 0. \tag{3.33}$$

Proof. Outside C_1: This follows the general case (Theorem 2.3) with one exception. Since $c_2 = 0$, there is no binomial series from the integral in (2.10) when $\zeta \in C_2$. Thus

$$a_{1,-(k+1)} - \rho_2^{k+1} a_{2,-(k+1)} - \sum_{\nu=3}^{m} \sum_{j=0}^{k} \binom{k}{j} \rho_\nu^{j+1} c_\nu^{k-j} a_{\nu,-(j+1)} = 0.$$

Inside C_2: For any z in the interior of D_2 and $\zeta \in C$ it is clear that $\frac{|z-c_2|}{|\zeta-c_2|} < 1$. But $c_2 = 0$ and so this is just $\frac{|z|}{|\zeta|} < 1$ which means

$$\frac{1}{2\pi i} \int_C f(\zeta) \zeta^{-k-1} \, d\zeta = 0,$$

and so

$$\rho_2^k a_{1,k} - a_{2,k} - \sum_{\nu=3}^{m} \sum_{j=0}^{\infty} \frac{\rho_2^k}{c_\nu^{k+1}} B_{k+1,j} \frac{\rho_\nu^{j+1}}{(-c_\nu)^j} a_{\nu,-(j+1)} = 0.$$

Inside C_ℓ ($\ell = 3, \ldots, m$): Again following the argument from the general case

$$\sum_{j=0}^{\infty} \rho_\ell^k B_{k+1,j} c_\ell^j a_{1,k+j} - a_{\ell,k} - \sum_{\substack{\nu=2 \\ \nu \neq \ell}}^{m} \sum_{j=0}^{\infty} \frac{\rho_\ell^k}{(c_\nu - c_\ell)^{k+1}} B_{k+1,j} \frac{\rho_\nu^{j+1}}{(c_\ell - c_\nu)^j} a_{\nu,-(j+1)} = 0.$$

□

3.4 Linearization

Linearization for application to the Newton-like method is similar to the non-annulus case. Here an extra condition is explicitly given to handle $c_2 = 0$. These are again

$$(f + \delta f)(e^{i\theta}) = \xi_1(\theta) + \eta_\nu(\theta)U_1(\theta), \tag{3.34}$$

$$(f + \delta f)(\rho_2 e^{i\theta}) = \xi_2(\theta) + \eta_2(\theta)U_2(\theta) + \zeta_2(\theta)(\delta\rho_2), \tag{3.35}$$

and

$$(f + \delta f)(c_\nu + \rho_\nu e^{i\theta}) = \xi_\nu(\theta) + \eta_\nu(\theta)U_\nu(\theta) + \zeta_\nu(\theta)(\delta\rho_\nu + \delta c_\nu e^{-i\theta}) \tag{3.36}$$

where ξ_ν, η_ν, and ζ_ν are defined as before.

3.5 Discretization and matrix formation

Normalization is done in such a way that no extra conditions are needed. Then limiting again the system of equations dictated by the analyticity conditions (3.31), (3.32), and (3.33) to $M = N/2$ equations and M terms the discrete form of these become

$$a_{1,-(k+1)} - \rho_2^{k+1} a_{2,-(k+1)} - \sum_{\nu=3}^{m}\sum_{j=0}^{k} \binom{k}{j} \rho_\nu^{j+1} c_\nu^{k-j} a_{\nu,-(j+1)} = 0, \tag{3.37}$$

$$\rho_2^k a_{1,k} - a_{2,k} - \sum_{\nu=3}^{m}\sum_{j=0}^{M-1} \frac{\rho_2^k}{c_\nu^{k+1}} B_{k+1,j} \frac{\rho_\nu^{j+1}}{(-c_\nu)^j} a_{\nu,-(j+1)} = 0, \tag{3.38}$$

and

$$\sum_{j=0}^{M-1} \rho_\ell^k B_{k+1,j} c_\ell^j a_{1,k+j} - a_{\ell,k} - \sum_{\substack{\nu=2 \\ \nu\neq\ell}}^{m}\sum_{j=0}^{M-1} \frac{\rho_\ell^k}{(c_\nu - c_\ell)^{k+1}} B_{k+1,j} \frac{\rho_\nu^{j+1}}{(c_\ell - c_\nu)^j} a_{\nu,-(j+1)} = 0. \tag{3.39}$$

Written in matrix form this is

$$P\underline{a} = P_1\underline{a}_1 + \cdots + P_m\underline{a}_m = [P_1 \quad \cdots \quad P_m] \begin{bmatrix} \underline{a}_1 \\ \vdots \\ \underline{a}_m \end{bmatrix} = 0, \tag{3.40}$$

and the P matrices have the block structure

$$P_1 = \begin{bmatrix} 0 & I \\ I_+^{\rho_2^k} & 0 \\ P_{3,1} & 0 \\ \vdots & \vdots \\ P_{m,1} & 0 \end{bmatrix} \qquad P_2 = \begin{bmatrix} 0 & -I_-^{\rho_2^{k+1}} \\ -I & 0 \\ 0 & -P_{3,2} \\ \vdots & \vdots \\ 0 & -P_{m,2} \end{bmatrix} \qquad \underset{(\nu \geq 3)}{P_\nu} = \begin{bmatrix} 0 & -P_{1,\nu} \\ \vdots & \vdots \\ 0 & -P_{\nu-1,\nu} \\ -I & 0 \\ 0 & -P_{\nu+1,\nu} \\ \vdots & \vdots \\ 0 & -P_{m,\nu} \end{bmatrix}$$

where $I_+^{\rho_2^k} = \operatorname{diag}\left(\rho_2^{(0:M-1)}\right)$, $I_-^{\rho_2^{k+1}} = \operatorname{diag}\left(\rho_2^{(M:-1:1)}\right)$, and each submatrix is $M \times M$. For the details of the submatrices see Appendix A.

For ease of exposition we assume that m=4 for the rest of this section. The vectored form of the linearization conditions are then

$$\begin{aligned} N\underline{a}_1 &= F\underline{\xi}_1 + FE_1\underline{U}_1 \\ N\underline{a}_2 &= F\underline{\xi}_2 + FE_2\underline{U}_2 + \delta\rho_2 F\underline{\zeta}_2 \\ N\underline{a}_3 &= F\underline{\xi}_3 + FE_3\underline{U}_3 + \delta\rho_3 F\underline{\zeta}_3 + \operatorname{Re}\delta c_3 F(\underline{q} * \underline{\zeta}_3) \\ N\underline{a}_4 &= F\underline{\xi}_4 + FE_4\underline{U}_4 + \delta\rho_4 F\underline{\zeta}_4 + \delta c_4 F(\underline{q} * \underline{\zeta}_4) \end{aligned}$$

which in combination with (3.40) leads to

$$\begin{aligned} P_1 FE_1\underline{U}_1 &+ P_2(FE_2\underline{U}_2 + \delta\rho_2 F\underline{\zeta}_2) \\ &+ P_3(FE_3\underline{U}_3 + \delta\rho_3 F\underline{\zeta}_3 + \operatorname{Re}\delta c_3 F(\underline{q} * \underline{\zeta}_3)) \\ &+ P_4(FE_2\underline{U}_4 + \delta\rho_4 F\underline{\zeta}_4 + (\operatorname{Re}\delta c_4 + i\operatorname{Im}\delta c_4)F(\underline{q} * \underline{\zeta}_4)) \\ &= -P_1 F\underline{\xi}_1 - P_2 F\underline{\xi}_2 - P_3 F\underline{\xi}_3 - P_4 F\underline{\xi}_4 := g. \end{aligned}$$

So with

$$P = \begin{bmatrix} P_1 & P_2 & P_3 & P_4 \end{bmatrix}, \quad \text{and} \quad W = \begin{bmatrix} \underline{w}_2 & \underline{w}_3 & \underline{w}_4 & \underline{wq}_3 & \underline{wq}_4 & i\underline{wq}_4 \end{bmatrix}$$

where $\underline{w}_\nu := P_\nu F\underline{\zeta}_\nu$ and $\underline{wq}_\nu := P_\nu F(\underline{q} * \underline{\zeta}_\nu)$, and the $(4N+6)\times 1$ vector

$$\underline{U} = \begin{bmatrix} \underline{U}_1^T & \underline{U}_2^T & \underline{U}_3^T & \underline{U}_4^T & \delta\rho_2 & \delta\rho_3 & \delta\rho_4 & \mathrm{Re}\,\delta c_3 & \mathrm{Re}\,\delta c_4 & \mathrm{Im}\,\delta c_4 \end{bmatrix}^T,$$

the linear system can now be written

$$D\underline{U} := \begin{bmatrix} P_1 & P_2 & P_3 & P_4 & W \end{bmatrix} \begin{bmatrix} FE_2 & 0 & 0 & 0 & 0 \\ 0 & FE_2 & 0 & 0 & 0 \\ 0 & 0 & FE_3 & 0 & 0 \\ 0 & 0 & 0 & FE_4 & 0 \\ 0 & 0 & 0 & 0 & I \end{bmatrix} \underline{U} = \underline{g}. \tag{3.41}$$

Using the "normal equations" and the fact $\underline{U}$ is real, the vector $\underline{U}$ in the system

$$A\underline{U} := \frac{2}{N}\mathrm{Re}\,(D^H D)\underline{U} = \frac{2}{N}\mathrm{Re}\,(D^H g) := b \tag{3.42}$$

can be found using the conjugate gradient method.

3.6 Analysis of the linear system

Consider the matrix A in (3.42),

$$A = \frac{2}{N}\mathrm{Re}\,(D^H D) = \begin{bmatrix} A_{11} & A_{12} & A_{13} & A_{14} & X_1 \\ A_{21} & A_{22} & A_{23} & A_{24} & X_2 \\ A_{31} & A_{32} & A_{33} & A_{34} & X_3 \\ A_{41} & A_{42} & A_{43} & A_{44} & X_4 \\ X_1^T & X_2^T & X_3^T & X_4^T & W^H W \end{bmatrix},$$

where $A_{kj} := (2/N)\mathrm{Re}\,(E_k^H F^H P_k^H P_j F E_j)$ and $X_k := (2/N)\mathrm{Re}\,(E_k^H F^H P_k^H W)$. Again it suffices to examine the submatrix

$$\hat{A} = \begin{bmatrix} A_{11} & A_{12} & A_{13} & A_{14} \\ A_{21} & A_{22} & A_{23} & A_{24} \\ A_{31} & A_{32} & A_{33} & A_{34} \\ A_{41} & A_{42} & A_{43} & A_{44} \end{bmatrix}$$

to address the eigenvalue distribution. By (3.40) and (3.5)

$$P = \begin{bmatrix} P_1 & P_2 & P_3 & P_4 \end{bmatrix} = \begin{bmatrix} 0 & I & 0 & -I_-^{\rho_2^{k+1}} & 0 & -P_{13} & 0 & -P_{14} \\ I_+^{\rho_2^k} & 0 & -I & 0 & 0 & -P_{23} & 0 & -P_{24} \\ P_{31} & 0 & 0 & -P_{32} & -I & 0 & 0 & -P_{34} \\ P_{41} & 0 & 0 & -P_{42} & 0 & -P_{43} & -I & 0 \end{bmatrix},$$

This implies

$$P^H P = \begin{bmatrix} P_1^H P_1 & P_1^H P_2 & P_1^H P_3 & P_1^H P_4 \\ P_2^H P_1 & P_2^H P_2 & P_2^H P_3 & P_2^H P_4 \\ P_3^H P_1 & P_3^H P_2 & P_3^H P_3 & P_3^H P_4 \\ P_4^H P_1 & P_4^H P_2 & P_4^H P_3 & P_4^H P_4 \end{bmatrix},$$

and the submatrix $P_1^H P_1$ is then

$$P_1^H P_1 = \begin{bmatrix} (I_+^{\rho_2^k})^2 + P_{31}^H P_{31} + P_{41}^H P_{41} & 0 \\ 0 & I \end{bmatrix}$$

$$= \begin{bmatrix} (I_+^{\rho_2^k})^2 + P_{31}^H P_{31} + P_{41}^H P_{41} & 0 \\ 0 & 0 \end{bmatrix} + \begin{bmatrix} 0 & 0 \\ 0 & I \end{bmatrix} := \Lambda_1 + I_-.$$

Rewriting A_{11},

$$A_{11} = A_{11}^{(1)} + A_{11}^{(2)} := (2/N)\mathrm{Re}\,(E_1^H F^H \Lambda_1 F E_1) + (2/N)\mathrm{Re}\,(E_1^H F^H I_- F E_1).$$

The rest of the analysis follows that given in the previous chapter.

3.7 Numerical examples

Example 3.1. The first example is again the identity map (Figure 3.10), $m = 4$. Accuracy of the map with perturbed initial guesses is given in Table 3.4.

	Accuracy	
N	centers	radii
32	10^{-8}	10^{-8}
64	10^{-12}	10^{-12}
128	10^{-13}	10^{-14}
256	10^{-16}	10^{-16}

Table 3.4: Identity map accuracy.

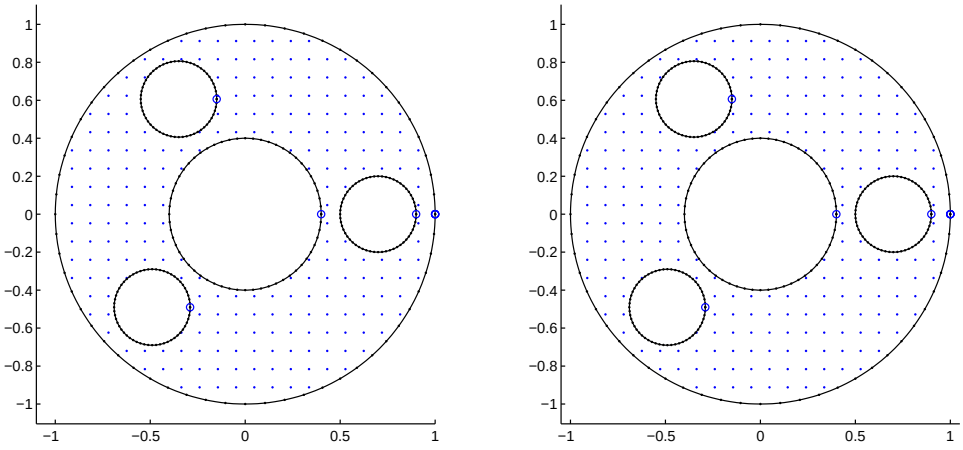

Figure 3.10: An identity map (Example 3.1).

Example 3.2. In this example (Figure 3.11), $m = 3$ and $M = 256$, the current case is applied to the target region used in Example 2.4. The number of Newton iterations reached the limit set at 20, and the last update had a magnitude of 10^{-12}.

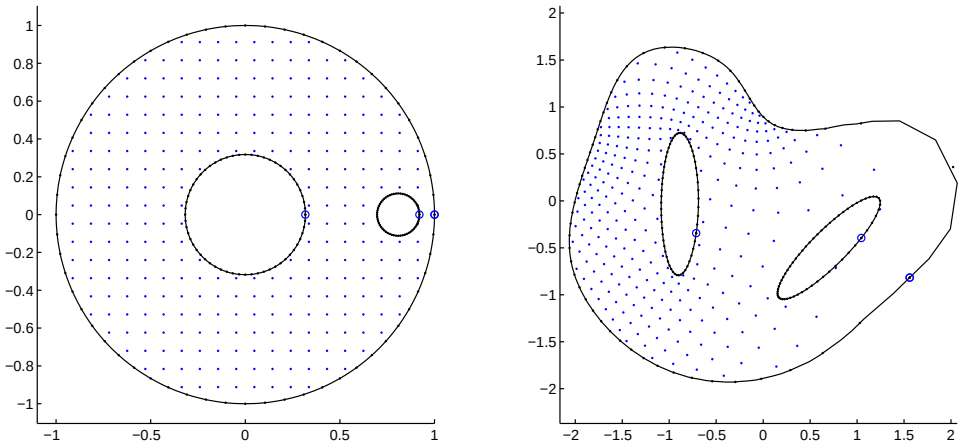

Figure 3.11: A target region with a spline outer boundary, $N = 256$ (Example 3.2).

Example 3.3. An example of connectivity $m = 6$ (Figure 3.12), $N = 128$. It should be noted that this was a difficult example to create. We have discovered that the annulus case introduces unwanted numeric distortions into the map when solving for regions which are not already somewhat annulus-shaped from the start. As more holes were added to this example, it was necessary to make them smaller in order to get a map that would converge.

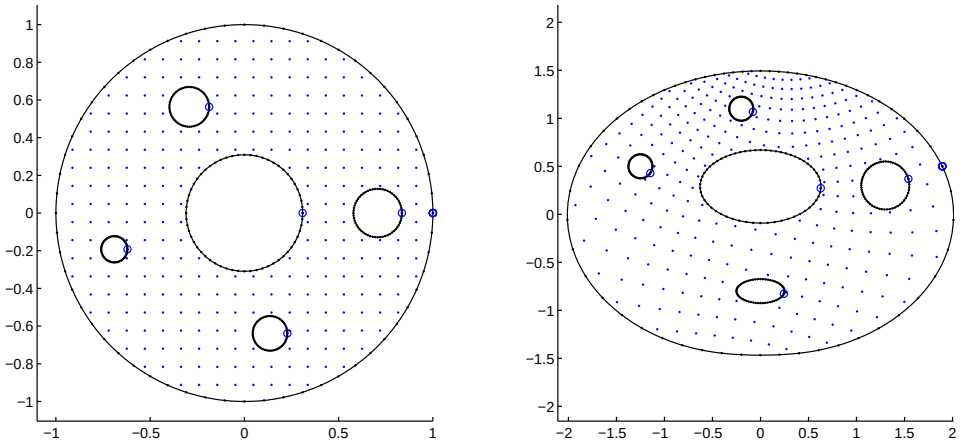

Figure 3.12: Connectivity $m = 6$, $N = 128$ (Example 3.3).

As for the generalized case, the nullspace for the matrix A for the above examples is given in Table 3.5. Note that for example 3.2 the range of the number of eigenvalues

Example	m	N	# $\lambda_i < \varepsilon_{\text{mach}}$	# $\lambda_i < 10\varepsilon_{\text{mach}}$
1	4	32	3-5	9
1	4	64	6-9	12
1	4	128	12	12
1	4	256	12	12
2	3	128	6-3	6-4
3	6	128	13-15	15

Table 3.5: Number of zero eigenvalues in the examples.

listed is in decreasing order. The observed behavior for this example is that the number of eigenvalues smaller than $\varepsilon_{\text{mach}}$ actually decreased as the Newton iterations increased. This was the only example where this behavior was observed. Again this eigenvalue behavior is unexplained and will be a part of future work.

CHAPTER 4

CONCLUSION

4.1 Concluding remarks

The main goal of this project was to revise the Fornberg-like method for the unbounded case presented in [3] to a Fornberg-like method for the bounded case. This was accomplished as presented in this thesis, and numerically in MATLAB. Two methods were presented, the general case and the annulus with circular holes case. It seems the annulus formulation is disadvantageous numerically, as it may in general introduce unnecessary distortion into the mapping function.

4.2 Future work

Although the main goal was accomplished, there is yet work to be done. Analytically an outstanding question is that of the nullspace of the matrix A. This nullspace was discussed as an observed phenomenon in the numeric examples, but is yet unexplained. The MATLAB code, though functional, also needs work.

Currently a matrix-matrix multiplication ($D^H D$) is performed to get the matrix A, and then CG is applied. A modification of CG is needed so that it is not necessary to actually perform $D^H D$. Thus if we could reduce the matrix-matrix multiplications to only matrix-vector multiplications it might be possible to have the entire algorithm perform on the order of $O(N^2)$.

When computing the map it is necessary to calculate $S'_\nu(\theta)$ at each iteration. This is currently done by a one-sided, finite difference approximation, but a better way would be through N-point trigonometric interpolation. The finite difference approximation gives

an accuracy of only $O(1/N)$ for S'_ν while a trigonometric interpolation would give spectral accuracy.

Initial guesses for the boundary correspondences $S_\nu(\theta)$ and the centers c_ν and radii ρ_ν are also not handled well by the current code. Currently, unless the target domain is "nearly" the circle domain in size and shape, the user must make these initial guesses manually.

REFERENCES

LIST OF REFERENCES

[1] L. Ahlfors. *Complex Analysis*. McGraw-Hill, 3rd edition, 1979.

[2] N. Benchama. *A Simplified Fornberg-like Method for the Conformal Mapping of Multiply Connected Regions*. PhD thesis, Wichita State University, December 2003.

[3] N. Benchama, T. DeLillo, T. Hrycak, and L. Wang. A simplified Fornberg-like method for the conformal mapping of multiply connected regions – comparisons and crowding. *J. Comput. Appl. Math.*, 209:1–21, 2007.

[4] T. DeLillo and A. Elcrat. A Fornberg-like conformal mapping method for slender regions. *Journal of Computational and Applied Mathematics*, 46(1-2):49–64, 1993.

[5] T. DeLillo, A. Elcrat, and J. Pfaltzgraff. Numerical conformal mapping methods based on Faber series. *Journal of Computational and Applied Mathematics*, 83(2):205–236, 1997.

[6] T. DeLillo, M. Horn, and J. Pfaltzgraff. Numerical conformal mapping of multiply connected regions by Fornberg-like methods. *Numerische Mathematik*, 83(2):205–230, 1999.

[7] T.K. DeLillo and J.A. Pfaltzgraff. Numerical conformal mapping methods for simply and doubly connected regions. *SIAM Journal on Scientific Computing*, 19:155, 1998.

[8] B. Fornberg. A numerical method for conformal mappings. *SIAM J. Sci. Stat. Comput*, 1(3):386–400, 1980.

[9] D. Gaier. *Konstruktive Methoden der Konformen Abbildung*. 1964.

[10] G. Golub and C. VanLoan. *Matrix Computations*. The Johns Hopkins University Press, 3 edition, 1996.

[11] P. Henrici. *Applied and Computational Complex Analysis*, volume III. Wiley, New York, 1986.

[12] M. Klonowska and W. Prosnak. On an effective method for conformal mapping of multiply connected domains. *Acta Mechanica*, 119(1):35–52, 1996.

[13] N. Muskhelishvili. *Singular Integral Equations*. Dover Publications, Inc., New York, 1992.

[14] Z. Nehari. *Conformal Mapping*. McGraw-Hill, New York, 1952.

[15] W. Prosnak. Conformal representation of arbitrary multiconnected airfoils. *Bull. Acad. Polish Sci.*, 25:25–36.

[16] W. Prosnak. *Computation of Fluid Motions in Multiply Connected Domains*. G. Braun, 1987.

[17] W. Rudin. *Functional Analysis*. McGraw-Hill, New York, 2nd edition, 1991.

[18] L. Wang. *Computational Methods for Two Problems in Potential Theory*. PhD thesis, Wichita State University, 2000.

[19] R. Wegmann. On Fornberg's numerical method for conformal mapping. *SIAM J. Numer. Anal.*, 23:1199–1213, 1986.

[20] R. Wegmann. Fast conformal mapping of an ellipse to a simply connected region. *Journal of Computational and Applied Mathematics*, 72(1):101–126, 1996.

[21] R. Wegmann. Fast conformal mapping of multiply connected regions. *Journal of Computational and Applied Mathematics*, 130(1-2):119–138, 2001.

[22] R. Wegmann. Methods for numerical conformal mapping. In R. Kuehnau, editor, *Handbook of Complex Analysis, Geometric Function Theory*, volume 2, pages 351–477. Elsevier, 2005.

[23] O. Widlund. On a numerical method for conformal mapping due to Fornberg. Unpublished, 1981.

APPENDICES

APPENDIX A

THE MATRIX P

Here the matrix P used in calculations in Chapters 2 and 3 is explained in greater detail. A comparison of the discrete analyticity conditions between the two cases presented in the text reveals that, ignoring some minor differences, the $M \times M$ submatrices are the same, and so the two cases will be presented together. For ease of exposition the generalized method from Chapter 2 will be referred to as the 'the general case' or 'the first case', while the annulus case with holes from Chapter 3 will be referenced as 'the annulus case' or 'the second case'.

Discretization of the analyticity conditions and the normalization conditions in the first case led to the linear system

$$a_{1,-(k+1)} - \sum_{\nu=2}^{m} \sum_{j=0}^{k} \binom{k}{j} \rho_\nu^{j+1} c_\nu^{k-j} a_{\nu,-(j+1)} = 0, \tag{A.43}$$

$$\sum_{j=0}^{M-1} B_{k+1,j} \rho_\ell^k c_\ell^j a_{1,k+j} - a_{\ell,k} - \sum_{\substack{\nu=2 \\ \nu \neq \ell}}^{m} \sum_{j=0}^{M-1} \frac{\rho_\ell^k}{(c_\nu - c_\ell)^{k+1}} B_{k+1,j} \frac{\rho_\nu^{j+1}}{(c_\ell - c_\nu)^j} a_{\nu,-(j+1)} = 0, \tag{A.44}$$

and

$$w_0 = f(z_0) = \sum_{j=0}^{M-1} a_{1,j} z_0^j + \sum_{\nu=2}^{m} \sum_{j=1}^{M} a_{\nu,-j} \left(\frac{\rho_\nu}{z_0 - c_\nu} \right)^j. \tag{A.45}$$

Written in matrix notation this is

$$P\underline{a} = P_1 \underline{a}_1 + \cdots + P_m \underline{a}_m = [P_1 \ \cdots \ P_m] \begin{bmatrix} \underline{a}_1 \\ \vdots \\ \underline{a}_m \end{bmatrix} = \begin{bmatrix} 0 \\ \vdots \\ 0 \\ w_0 \end{bmatrix} := \underline{r},$$

where each P_ν multiplies the corresponding coefficient vector a_ν. These have the block structure

$$P_1 = \begin{bmatrix} 0 & I \\ P_{2,1} & 0 \\ \vdots & \vdots \\ P_{m,1} & 0 \\ p_1 & 0 \end{bmatrix} \quad \text{and} \quad \underset{2\le\nu\le m}{P_\nu} = \begin{bmatrix} 0 & -P_{1,\nu} \\ \vdots & \vdots \\ 0 & -P_{\nu-1,\nu} \\ -I & 0 \\ 0 & -P_{\nu+1,\nu} \\ \vdots & \vdots \\ 0 & -P_{m,\nu} \\ 0 & -p_\nu \end{bmatrix}. \tag{A.46}$$

For the second case the discrete analyticity conditions were

$$a_{1,-(k+1)} - \rho_2^{k+1} a_{2,-(k+1)} - \sum_{\nu=3}^{m} \sum_{j=0}^{k} \binom{k}{j} \rho_\nu^{j+1} c_\nu^{k-j} a_{\nu,-(j+1)} = 0, \tag{A.47}$$

$$\rho_2^k a_{1,k} - a_{2,k} - \sum_{\nu=3}^{m} \sum_{j=0}^{M-1} \frac{\rho_2^k}{c_\nu^{k+1}} B_{k+1,j} \frac{\rho_\nu^{j+1}}{(-c_\nu)^j} a_{\nu,-(j+1)} = 0, \tag{A.48}$$

and

$$\sum_{j=0}^{M-1} \rho_\ell^k B_{k+1,j} c_\ell^j a_{1,k+j} - a_{\ell,k} - \sum_{\substack{\nu=2 \\ \nu\neq\ell}}^{m} \sum_{j=0}^{M-1} \frac{\rho_\ell^k}{(c_\nu - c_\ell)^{k+1}} B_{k+1,j} \frac{\rho_\nu^{j+1}}{(c_\ell - c_\nu)^j} a_{\nu,-(j+1)} = 0. \tag{A.49}$$

Written in matrix form this is

$$P\underline{a} = P_1\underline{a}_1 + \cdots + P_m\underline{a}_m = \begin{bmatrix} P_1 & \cdots & P_m \end{bmatrix} \begin{bmatrix} \underline{a}_1 \\ \vdots \\ \underline{a}_m \end{bmatrix} = 0,$$

and the P_ν matrices have the block structure

$$P_1 = \begin{bmatrix} 0 & I \\ I_+^{\rho_2^k} & 0 \\ P_{3,1} & 0 \\ \vdots & \vdots \\ P_{m,1} & 0 \end{bmatrix}, \qquad P_2 = \begin{bmatrix} 0 & -I_-^{\rho_2^{k+1}} \\ -I & 0 \\ 0 & -P_{3,2} \\ \vdots & \vdots \\ 0 & -P_{m,2} \end{bmatrix}, \qquad \underset{(\nu \geq 3)}{P_\nu} = \begin{bmatrix} 0 & -P_{1,\nu} \\ \vdots & \vdots \\ 0 & -P_{\nu-1,\nu} \\ -I & 0 \\ 0 & -P_{\nu+1,\nu} \\ \vdots & \vdots \\ 0 & -P_{m,\nu} \end{bmatrix} \tag{A.50}$$

where $I_+^{\rho_2^k} = \operatorname{diag}\left(\rho_2^{(0:M-1)}\right)$, $I_-^{\rho_2^{k+1}} = \operatorname{diag}\left(\rho_2^{(M:-1:1)}\right)$. The block structures then differ between the two cases only in the first two rows of P_1 and P_2. It turns out that computationally there is no difference between the $M \times M$ submatrices of the two cases.

Equation (A.43) or (A.47) determines the first block-row of each P_ν, so each $P_{1,\nu}$ has the form

$$\begin{bmatrix} \rho_\nu^M & \binom{M-1}{M-2}\rho_\nu^{M-1}c_\nu & \cdots & \binom{M-1}{1}\rho_\nu^2 c_\nu^{M-2} & \rho_\nu c_\nu^{M-1} \\ 0 & \rho_\nu^{M-1} & \cdots & \binom{M-2}{1}\rho_\nu^2 c_\nu^{M-3} & \rho_\nu c_\nu^{M-2} \\ \vdots & & \ddots & & \vdots \\ 0 & 0 & \cdots & \rho_\nu^2 & \rho_\nu c_\nu \\ 0 & 0 & \cdots & 0 & \rho_\nu \end{bmatrix}. \tag{A.51}$$

If one considers P_2 in the annulus case, then with $c_2 = 0$ the submatrix (A.51) reduces to exactly $I_-^{\rho_2^{k+1}}$. The structure of the submatrices, being nicely arranged binomial coefficients with convenient multiples of center and radii, is such that it is easy to code. The MATLAB code which produces submatrix (A.51) is given by Figure A.1. It is a modification of the method described in [2, Appendix A] used to calculate binomial coefficients while avoiding possible overflow or catastrophic cancellation.

```
% 1st block-row
P_=zeros(M);
P_(:,1) = rho*(c.^(0:M-1));
P_(:,2) = [0; rho*(1:M-1)'.*P_(1:M-1,1)];
for k=3:M
    for j=3:k
        P_(k,j) = rho*P_(k-1,j-1)*(k-1)/(j-1);
    end
end
Pnu(1:M,M+1:N) = -fliplr(flipud(P_));
```

Figure A.1: MATLAB code for submatrix (A.51).

The first term in (A.44) or (A.49) dictates interaction with the coefficients $\underline{a}_1$, which means each $P_{\nu,1}$ in P_1 takes the form

$$\begin{bmatrix} 1 & c_\nu & c_\nu^2 & c_\nu^3 & \cdots & c_\nu^{M-1} \\ 0 & \rho_\nu & 2\rho_\nu c_\nu & 3\rho_\nu c_\nu^2 & \cdots & B_{2,M-2}\rho_\nu c_\nu^{M-2} \\ \vdots & & \ddots & & \cdots & \vdots \\ \vdots & & & \ddots & \cdots & \vdots \\ 0 & & \cdots & & \rho_\nu^{M-2} & B_{M-1,1}\rho_\nu^{M-2}c_\nu \\ 0 & & \cdots & & 0 & \rho_\nu^{M-1} \end{bmatrix}. \tag{A.52}$$

However for the annulus case when $c_2 = 0$ the first term in equation (A.49) determines the form and the submatrix (A.52) reduces to $I_+^{\rho_2^k}$. The MATLAB code for this matrix is shown in Figure A.2.

The third term in (A.44), (A.48), or (A.49) drives the form of each $P_{\nu\neq\ell,\nu}$, which look like

$$\begin{bmatrix} \frac{1}{c_\nu - c_\ell}\frac{\rho_\nu^M}{(c_\ell - c_\nu)^{M-1}} & \cdots & \frac{1}{c_\nu - c_\ell}\rho_\nu \\ \vdots & \ddots & \vdots \\ \frac{\rho_\ell^{M-1}}{(c_\nu - c_\ell)^M}B_{M,M-1}\frac{\rho_\nu^M}{(c_\ell - c_\nu)^{M-1}} & \cdots & \frac{\rho_\ell^{M-1}}{(c_\nu - c_\ell)^M}B_{M,0}\rho_\nu \end{bmatrix}. \tag{A.53}$$

The MATLAB code to produce submatrix (A.53) is the most complicated, and is shown in Figure A.3. It has a computational cost of $O(N^2)$.

```
P_=zeros(M);
P_(:,1) = c.^(0:M-1);
P_(:,2) = [0; rho*(1:M-1)'.*P_(1:M-1,1)];
for k=3:M
    for j=3:k
        % (j-1)+(k-(j-1))-1 = (k-1)
        P_(k,j) = rho*P_(k-1,j-1)*(k-1)/(j-1);
    end
end
Pnu(L*M+1:(L+1)*M,1:M) = P_.';
```

Figure A.2: MATLAB code for submatrix (A.52), where `L+1` represents the block-row of P_1.

```
% pl is rho_l, pv is rho_v, cvl is (c_v-c_l), and clv
% is (c_l-c_v)
pl_cvl = pl/cvl;
P_(1,:) = (1/(cvl)*(pv.^(1:M)./(clv).^(0:M-1));
P_(2,:) = pl_cvl*(1:M).*(P_(1,:));
for k=3:M
    for j=1:M
        P_(k,j) = pl_cvl*P_(k-1,j)*(j+k-2)/(k-1);
    end
end
Pnu(L*M+1:(L+1)*M,M+1:N) = -fliplr(P_);
```

Figure A.3: MATLAB code to produce submatrix (A.53), where `L+1` is the current block-row of P_ν.

And finally, for the general case only, equation (A.45) specifies the submatrices p_1 through p_m. In P_1

$$p_1 = \begin{bmatrix} 1 & z_0 & \cdots & z_0^{M-1} \end{bmatrix}$$

and in each P_ν

$$p_\nu = \begin{bmatrix} \left(\frac{\rho_\nu}{z_0 - c_\nu}\right)^M & \cdots & \left(\frac{\rho_\nu}{z_0 - c_\nu}\right) \end{bmatrix}.$$

It should be noted that it is not necessary to actually form the matrix P. As is pointed out in the description of the algorithm, each P_ν is formed separately and then used to form D.

APPENDIX B

THE ALGORITHM

Here a short description of the algorithm used in the general case is presented as developed in MATLAB. The algorithm for the annulus case with circular holes is similar. The algorithm is fairly simple conceptually; it is presented step-by-step.

1. Given the target region, make initial guesses (or use those supplied by the user) of the centers, radii, and boundary correspondences.

   Creating a good initial guess algorithmically is still under development. The current incarnation of the code relies almost exclusively on user supplied data.

2. Start the Newton iteration.

3. Form the matrix D and vector $\underline{g}$.

   This is shown in Figure B.1. Note that the matrix P is never explicitly formed; we only need form each P_ν separately. On the first iteration the variables `P`, `c`, and `rho` are the initial guesses supplied by the user. The 1×3 array `norm_cond`, which represents the normalization conditions, is defined to be `norm_cond` $= \Big[f(1) \quad z_0 \quad f(z_0) \Big]$. The function `xi_eta` is supplied by the user and should return $\gamma_\nu(S_\nu(\underline{\theta}))$ and $\gamma'_\nu(S_\nu(\underline{\theta}))$ for all $1 \leq \nu \leq m$ as two $N \times m$ matrices. The function `make_Pnu` builds the submatrices P_ν as described in Appendix A. The variable `Sdiff` is the one-sided, finite difference approximation to S'_ν.

4. Form the matrix A, vector $\underline{b}$, and then solve $A\underline{U} = \underline{b}$ using CG.

```
U_row_sz = m*N + 3*(m-1);
D = zeros(m*M+2,U_row_sz);
U = zeros(U_row_sz,1);
p1 = [1 zeros(1,N-1)];
if norm_cond(2) ~= 0    % z_0 is non-zero
    p1(1,2:M) = norm_cond(2).^(1:M-1);
end
pnu = zeros(1,N);
q = exp(-1i*(0:N-1)'*2*pi/N);
tl = boundary_length; % 1xm vector of boundary lengths
[xi eta] = xi_eta(S);
abs_eta = abs(eta);
eta = eta./abs_eta;

% form system to solve
Pnu = [make_Pnu(1,m,c,rho,N); p1];
D(1:end-1,1:N) = Pnu*fft(diag(eta(:,1)));
g_ = -Pnu*fft(xi(:,1));
for nu=2:m
    pnu(M+1:N) = (rho(nu-1)(norm_cond(2)-c(nu-1))).^(M:-1:1);
    Pnu = [make_Pnu(nu,m,c,rho,N); pnu];
    D(1:end-1,(nu-1)*N+1:nu*N) = Pnu*fft(diag(eta(:,nu)));

    Sdiff = diff([S(:,nu);S(1,nu)+tl(nu)])*(N/(2*pi));
    zeta = 1i*(abs_eta(:,nu).*eta(:,nu).*Sdiff)/rho(nu-1);
    D(1:end-1,m*N+nu-1) = Pnu*fft(zeta);
    D(1:end-1,m*N+m+2*(nu-2)) = Pnu*fft(q.*zeta);
    D(1:end-1,m*N+m+2*(nu-2)+1) = 1i*D(1:end-1,m*N+m+2*(nu-2));
    g_ = g_ - Pnu*fft(xi(:,nu));
end

% add normalization conditions
D(end,:) = [1 zeros(1,m*N+3*(m-1)-1)];
g_(end) = g_(end) + obj.N*norm_cond(3);
g = [g_; 0];
```

Figure B.1: Forming the matrix D.

See Figure B.2. In the current version of the code we perform the matrix-matrix multiplication $D^H D$. An iterative solver which would not require this matrix product would yield an increase in efficiency.

```
A=2*real(D'*D)/N;
b=2*real(D'*g)/N;
U=cgm(A,b,cgm_options);
```

Figure B.2: Forming the matrix A and solving the linear system.

5. Apply the updates to the centers, radii, and boundary correspondences.

   This is shown in Figure B.3.

```
U = [U(1:m*N)./abs_eta(:) ; U(m*N+1:end)];
S = S + reshape(U(1:m*N),N,m);
rho = rho + U(m*N+1:m*N+m-1);
c = c + U(m*N+m:2:m*N+m+2*m-4) + 1i*U(m*N+m+1:2:m*N+m+2*m-2);
```

Figure B.3: Applying the Newton updates.

6. If $\|U\|_\infty$ is less than a set value or the Newton iterations have reached a maximum value, then stop. Otherwise do another Newton iteration.

7. Calculate the Fourier coefficients and form the map.

   The Fourier coefficients for the map (2.5) can be calculated by ignoring the updates in equations (2.27) and (2.28), that is $N\underline{a}_\nu = F\underline{\xi}_\nu$. See Figures B.4 and B.5.

```
xi = xi_eta(S);
a = zeros(N,m);
for nu=1:m
    a(:,nu) = fft(xi(:,nu))/N;
end
f = @(z) map_eval(z,a,c,rho);
```

Figure B.4: Setting the Fourier coefficients and forming the map.

```
function w = map_eval(z,a,c,rho)
    [N,m]=size(a);
    w = polyval(a(N/2:-1:1,1),z);
    for nu=2:m
        w = w + polyval([a(N/2+1:N,nu);0],
                            rho(nu-1)./(z-c(nu-1)));
    end
end
```

Figure B.5: The map evaluation function.